JCI The Journal of Clinical Investigation

HIC1 deletion promotes breast cancer progression by activating tumor cell/fibroblast crosstalk

Yingying Wang, Xiaoling Weng, Luoyang Wang, Mingang Hao, Yue Li, Lidan Hou, Yu Liang, Tianqi Wu, Mengfei Yao, Guowen Lin, Yiwei Jiang, Guohui Fu, Zhaoyuan Hou, Xiangjun Meng, Jinsong Lu, Jianhua Wang

J Clin Invest. 2018. https://doi.org/10.1172/JCI99974.

Research In-Press Preview **Cell biology** **Oncology**

Graphical abstract

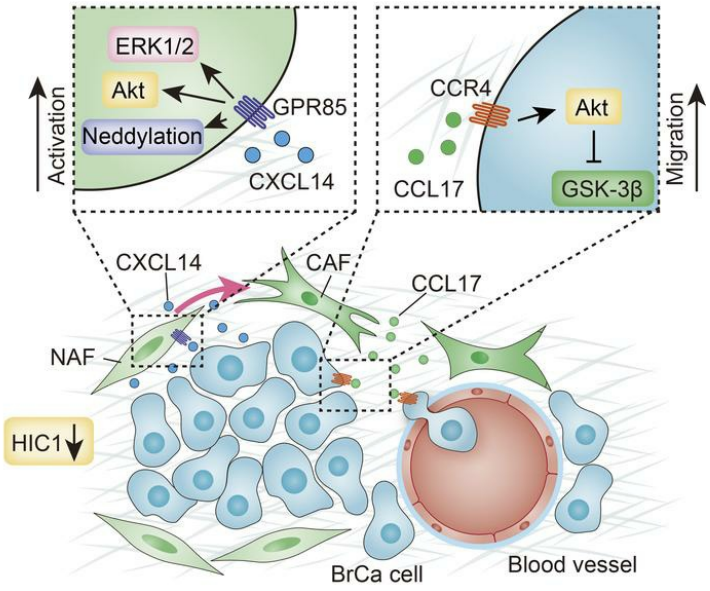

HIC1 deletion promotes breast cancer progression by activating tumor cell/fibroblast crosstalk

Yingying Wang[1], Xiaoling Weng[8], Luoyang Wang[2], Mingang Hao[3], Yue Li[4], Lidan Hou[5], Yu Liang[5], Tianqi Wu[8], Mengfei Yao[8], Guowen Lin[7], Yiwei Jiang[6], Guohui Fu[4], Zhaoyuan Hou[1*], Xiangjun Meng[5*], Jinsong Lu[6*], Jianhua Wang[8,9,10*].

[1]Department of Biochemistry and Molecular Cell Biology, Shanghai Jiao Tong University School of Medicine, Shanghai, China.

[2]Department of Chemical Engineering, Tsinghua University, Beijing, China.

[3]Department of Cancer Biology, University of Cincinnati College of Medicine, Cincinnati, USA.

[4]Pathology Center, Shanghai First People's Hospital, Shanghai Jiao Tong University School of Medicine, Shanghai, China.

[5]Department of Gastroenterology, Shanghai ninth People's Hospital, Shanghai Jiao Tong University School of Medicine, Shanghai, China.

[6]Department of Breast Surgery, Renji Hospital, Shanghai Jiao Tong University School of Medicine, Shanghai, China.

[7]Department of Urology, Fudan University Shanghai Cancer Center, Fudan University, Shanghai, China.

[8]Cancer institute, Fudan University Shanghai Cancer Center, Fudan University, Shanghai, China;

[9]School of Medicine, Anhui University of Science & Technology, Huainan, Anhui, China.

[10]Lead contact

*Corresponding authors at: Cancer Institute, Fudan University Shanghai Cancer Center, Fudan University, Shanghai, China (J. Wang), Tel: 0086-21-54660871.

E-mail addresses: jianhuaw2007@qq.com (J. Wang), lujjss@163.com (J. Lu), meng_xiangjun@yahoo.com (X. Meng), houzy@sjtu.edu.cn (Z. Hou).

Conflict of interest statements

The authors have declared that no conflict of interest exists

Running title

HIC1 deletion-mediated crosstalk and breast cancer progression

Abstract

Breast cancer (BrCa) is the malignant tumor that most seriously threatens female health; however, the molecular mechanism underlying its progression remains unclear. Here, we found that conditional deletion of HIC1 in the mouse mammary gland might contribute to premalignant transformation in the early stage of tumor formation. Moreover, the chemokine CXCL14 secreted by HIC1-deleted BrCa cells bound to its novel cognate receptor GPR85 on mammary fibroblasts in the microenvironment and was responsible for activating these fibroblasts via the ERK1/2, Akt, and neddylation pathways, whereas the activated fibroblasts promoted BrCa progression via the induction of the epithelial–mesenchymal transition (EMT) by the CCL17/CCR4 axis. Finally, we confirmed that the HIC1-CXCL14-CCL17 loop was associated with the malignant progression of BrCa. Therefore, the crosstalk between HIC1-deleted BrCa cells and mammary fibroblasts might play a critical role in BrCa development. Taken together, exploring the progression of BrCa from the perspective of microenvironment will be beneficial for identifying the potential prognostic marker of breast tumor and providing the more effective treatment strategy.

Keywords: Breast cancer, HIC1, CXCL14, CCL17

Introduction

Breast cancer (BrCa) is the most frequently diagnosed malignant tumor in women worldwide and represents the main cause of cancer-related death (1). Although systematic therapeutic approaches have decreased cancer-specific mortality, BrCa is still associated with high rates of cancer recurrence and metastasis (2). Therefore, exploring the mechanism underlying BrCa progression may be beneficial for diagnosis and treatment of the disease.

Recently, increasing evidence has shown that an appropriate tumor microenvironment (the soil) is necessary for the optimal growth of tumor cells (the seed) (3, 4). The tumor microenvironment includes various types of stromal cells that play a pivotal role in cancer progression (4). Among these cells, cancer-associated fibroblasts (CAFs) are the most abundant cell type involved in tumor development, orchestrating proliferation, invasion and neoangiogenesis (5, 6). Notably, CAFs exhibit a mesenchymal-like phenotype and promote the metastasis of both premalignant and malignant mammary epithelial cells in BrCa (7). It is well accepted that CAFs are mainly derived from normal-associated fibroblasts (NAFs) and that they are induced by cancer-secreted cytokines such as TGF-β and CXCL12/SDF-1 (8) or by loss of the expression of tumor suppressor genes such as *PTEN*, *TP53*, *CDKN1A* and *CAV1* (9-13). Reciprocally, the activated CAFs can cause BrCa epithelial cells to progress to more malignant stages (6, 14). Since it is accepted that the stroma is more genetically stable than cancerous epithelial cells, targeting the collateral interactions of CAFs may offer therapies that are less prone to the development of resistance. Therefore, focusing on the role and mechanism of CAFs in BrCa may provide a novel strategy for the treatment of BrCa patients.

Hypermethylated in cancer 1 (*HIC1*) is a tumor suppressor gene located at 17p13.3. *HIC1* resides completely within a CpG island that is frequently hypermethylated in human tumors, including breast, prostate and lung cancer (15-17). HIC1 is located close to telomeric TP53, which is a sequence-specific transcriptional repressor belonging to the BTB/POZ and C2H2 zinc finger family (18). The N-terminal BTB/POZ domain of HIC1 is responsible for protein–protein interactions that are crucial for its biological function, and the C-terminal zinc finger domains are involved in sequence-specific binding to an HIC1-responsive element (HiRE) with a TGCC or GGCA core motif (19, 20). It has been reported that epigenetic silencing of *HIC1* is one of the most common events in human cancer (15, 16, 21). Moreover, conventional knockout mice with homozygous deletion of *HIC1* display embryonic lethality at mid-gestation (22), whereas heterozygous mutants develop a range of spontaneous tumors in an age-dependent manner (23). As a transcription factor, several downstream target genes of HIC1 have been identified; these include *ACKR3*, *CXCR4*, *EFNA1*, *SNAI2*, *SIRT1* and *IL6*, which are associated with the modulation of angiogenesis, proliferation and metastasis (16, 19, 21, 24-26). In previous work, we showed that HIC1 expression is silenced only in highly malignant triple-

negative breast cancer (TNBC) compared with other molecular subtypes of BrCa and that this silencing induces autocrine secretion of LCN2 that facilitates BrCa progression (21). However, the role and mechanism underlying the effect of HIC1 loss on modulation of the tumor microenvironment remain unsettled, but they are crucial to exploring the function of HIC1 in BrCa progression.

Results

HIC1 deletion induces hyperplasia and lactogenic defects in mammary gland in vivo

Although our previous work indicated that HIC1 is silenced in some human cancers, including TNBC (16, 21, 26), its intrinsic role and the mechanism of its action in BrCa progression remain unknown. Here, to investigate the role of HIC1 in mammary gland malignant development in vivo, we generated *Hic1*$^{-/-}$ conditional knockout mice by crossing *Hic1*$^{fl/fl}$ mice with *Wap-Cre* mice in which Cre recombinase expression is driven by the mammary-specific whey acidic protein (*Wap*) promoter, which is activated at mid-pregnancy in luminal epithelial cells. The Cre-positive *Hic1*$^{fl/fl}$ mice were used as the *Hic1*$^{-/-}$ group, and their Cre-negative *Hic1*$^{fl/fl}$ littermates, which were designated *Hic1*$^{+/+}$, were used as controls (Supplemental Figure 1A). Western blot and RT-qPCR assays indicated that HIC1 deletion occurred only in mammary epithelium and not in liver, lung or muscle (Supplemental Figure 1B). Notably, using whole-mount staining at 4 M, 8 M and 12 M mice, we found striking hyperplastic abnormalities in the mammary ductal trees of *Hic1*$^{-/-}$ mice compared with their *Hic1*$^{+/+}$ littermates (Figure 1A and Supplemental Figure 1C). Similarly, H&E-stained sections of the animals' mammary glands showed that the epithelial layers in *Hic1*$^{-/-}$ mice were thicker than those in *Hic1*$^{+/+}$ mice (Figure 1B). This effect was largely due to an increased population of epithelial cells. This was confirmed by immunofluorescence staining showing marked expression of the luminal marker keratin 8 (K8) (Figure 1C). In addition, greatly increased numbers of proliferative cells were observed in *Hic1*$^{-/-}$ mice compared with controls using Ki67 and cyclin D1 staining (Figure 1D). Moreover, deletion of HIC1 in MCF7 luminal BrCa cells increased their ability to form vasculogenic networks on matrigel (Supplemental Figure 1G and Figure 2B). In contrast, restoration of HIC1 expression in MDA-MB-231 TNBC cells had the opposite effect (Supplemental Figure 1H). These findings indicate that HIC1 deletion may be associated with the premalignant development of mammary gland tissue.

Unexpectedly, we observed that pups born to *Hic1*$^{-/-}$ dams had lower weights than those reared by *Hic1*$^{+/+}$ dams, although their 48 h survival rates did not differ (Supplemental Figure 1D). This suggested that profound lactogenic defects might be present in *Hic1*$^{-/-}$ dams. Mammary gland whole mounts obtained from *Hic1*$^{-/-}$ dams at L6 were smaller than those obtained from controls (Supplemental Figure 1C), indicating a deficiency in the amounts of secretory products. H&E staining of mammary glands showed the presence of lipid droplets in *Hic1*$^{+/+}$ dams (red arrows), whereas the *Hic1*$^{-/-}$ glands contained very few lipid droplets (Supplemental Figure 1E). Oil-Red O staining further indicated that the alveoli of *Hic1*$^{-/-}$ glands did not contain significant quantities of milk fat (Supplemental Figure 1F). These data suggest that HIC1 deletion also induces lactogenic defects in mammary glands in vivo.

Finally, based on the data in the TCGA database, we observed that *HIC1* mRNA levels were significantly lower in BrCa tissues than in normal tissues from the same patients in 113 cases (Figure 1E). Consistent with

our previous results (21), *HIC1* mRNA levels were lower in 123 TNBC cases than in 972 non-TNBC patients in the TCGA database (Figure 1E). Furthermore, the expression of *HIC1* was also observed to be decreased in high-grade BrCa tissues compared with low-grade tissues both in the TCGA database and in an Oncomine dataset (Zhao Breast) (Figure 1E and Supplemental Figure 1I). Using the Kaplan-Meier method followed by the log-rank test, we further confirmed that HIC1 deletion correlates with lower relapse-free survival (Figure 1F) (27). These data suggest that HIC1 deletion is associated with poor prognosis of BrCa.

HIC1-deleted BrCa cells induce the activation of stromal fibroblasts in mammary gland

It has been reported that HIC1 deletion may play a role in modulating the stromal microenvironment by causing stromal cells to secrete specific factors (16, 21). We explored whether HIC1-deleted mammary gland epithelial cells have the ability to affect stromal fibroblasts. Notably, $Hic1^{-/-}$ mice were found to have markedly activated fibroblasts in their mammary gland stroma compared with $Hic1^{+/+}$ mice based on an evaluation of the expression of α-smooth muscle actin (α-SMA), which is frequently used as a classical marker of CAF in solid tumors (8, 28) (Figure 2A). To confirm this effect in vitro, HIC1-deleted MCF7 and T47D luminal BrCa cells (hereinafter referred to as $MCF7^{Ctrl}$/$MCF7^{sgHIC1}$ or $T47D^{Ctrl}$/$T47D^{sgHIC1}$) were obtained using the CRISPR-Cas9 system (Figure 2B), and primary mammary fibroblasts were freshly isolated from 4 human BrCa central and peripheral tumor areas (denoted as CAFs or NAFs, respectively) (Figure 2C). Figure 2C shows that the expression of α-SMA was higher in CAF2, 6, 8 and 10 than it was in the respective NAFs, albeit the expression of the other two CAF markers, fibroblast activation protein (FAP) and platelet-derived growth factor receptor α (PDGFRα), did not follow the same trend. Next, a co-culture system was used to simulate the in vivo situation. In this system, primary NAFs were placed in the lower chambers of a transwell apparatus, and $MCF7^{Ctrl}$/$MCF7^{sgHIC1}$ or $T47D^{Ctrl}$/$T47D^{sgHIC1}$ cells were re-plated in the upper chambers (Figure 2D). After 4 days, we performed Western blot assays and immunofluorescence staining and found that, compared with the respective controls, expression of the CAF markers, especially α-SMA, was dramatically increased in NAF6 cells that were co-cultured with $MCF7^{sgHIC1}$/$T47D^{sgHIC1}$ cells; the phenotypes of the cells were highly similar to those of primary CAFs (Figure 2E and 2F). Together, these data suggest that HIC1-deleted BrCa cells can directly induce the activation of stromal fibroblasts in mammary gland in vivo and in vitro.

***CXCL14* is a direct target gene of HIC1**

Next, to identify potential downstream targets of HIC1, we analyzed the published data on the genome-wide transcriptome profiles of MDA-MB-231^{HIC1}/MDA-MB-231^{GFP} and HBL-100^{shHIC1}/HBL-100^{shNC} cells using Agilent Whole Human Genome Microarrays (21) (Supplemental Figure 2A). Among the differentially expressed genes encoding cytokines, eight genes that may participate in the activation of mammary fibroblasts

were identified (Figure 3A and Supplemental Figure 2B). RT-qPCR was performed to assay the expression of these eight genes at the mRNA level in MCF7^{sgHIC1}/MCF7^{Ctrl}, T47D^{sgHIC1}/T47D^{Ctrl} and MDA-MB-231^{HIC1}/MDA-MB-231^{GFP} cells. Chemokine CXCL14 was chosen as a potentially relevant cytokine based on results showing that altering HIC1 expression in these cells markedly modulated CXCL14 expression at both the mRNA and protein levels compared with the controls (Figure 3A and 3B, and Supplemental Figure 2B). CXCL14 expression was also greatly increased in *Hic1*$^{-/-}$ mice at the mRNA and protein levels (Figure 3A and Supplemental Figure 2C). Similarly, the expression of *Sirt1*, a classical downstream gene of HIC1, was also observed to be enhanced in *Hic1*$^{-/-}$ mice (Figure 3A). These findings suggest that CXCL14 expression is modulated by HIC1.

Given that HIC1 functions as a repressive transcription factor and directly binds to the promoter regions of target genes (20), we inferred that *CXCL14* is a potential downstream target induced by HIC1. Indeed, as shown in Figure 3C, 11 putative HIC1-binding sites (TGCC/GGCA) were identified in the *CXCL14* promoter. We constructed a series of *CXCL14*-truncated promoter/reporter fusion plasmids containing progressive deletions of the 5' region of the gene from -2000 to +136 (Figure 3C). These constructs were then transfected together with the pcDNA3.1-His or the pcDNA3.1-HIC1 expression vector into 293T and MCF7 cells, and the promoter activities were measured using luciferase reporter assays. Figure 3D shows that when transfected into 293T and MCF7 cells, the construct containing the full-length *CXCL14* promoter resulted in higher activity than the basic construct. Moreover, transient transfection of the cells with HIC1 markedly inhibited *CXCL14* promoter activity (Figure 3D) in a dose-dependent manner (Supplemental Figure 2D). The inhibitory effect of HIC1 on *CXCL14* promoter activity in both cell lines was maintained in all the truncated constructs, including -2000/+136, -726/+136, -276/+136, and -41/+136 (Figure 3E). These results suggest that the regulatory region in the HIC1-mediated repression may be located within the -41 bp to +136 bp region of the *CXCL14* promoter, which contains two putative HIC1 binding sites, M1 and M2 (Supplemental Figure 2E). We mutated both sites (GGGCA to AAATG) to abolish HIC1 binding (Supplemental Figure 2E). Supplemental Figure 2F shows that only the construct in which site M1 was mutated significantly decreased the repressive capacity of HIC1, suggesting that the putative M1 site in the *CXCL14* promoter is essential for the HIC1-mediated inhibitory effect on *CXCL14* expression. Finally, to further determine whether the *CXCL14* promoter is indeed directly bound by HIC1, ChIP assays were performed in MCF7 and T47D cells using an antibody against HIC1. The pulled-down DNA was amplified by ordinary PCR and RT-qPCR (Figure 3F) with primers that were designed based on the -41/+136 region of the *CXCL14* promoter (Supplemental Figure 2E, underlined sequences). As shown in Figure 3F, the *CXCL14* promoter was markedly enriched in the HIC1-immunoprecipitated MCF7 and T47D chromatin but absent from the chromatin that was immunoprecipitated by the control rabbit IgG. Taken together, these results demonstrate that HIC1 directly

represses *CXCL14* transcription.

CXCL14 derived from HIC1-deleted BrCa cells mediates the activation of mammary fibroblasts

To explore whether CXCL14 activates mammary fibroblasts, various concentrations of rhCXCL14 were used to treat the primary mammary fibroblasts NAF2 and NAF6 cells. Western blot assays and immunofluorescence staining showed that NAF2 and NAF6 cells were markedly activated after the treatment with rhCXCL14; the phenotypes of the treated cells were very similar to those of the primary corresponding CAF2 and CAF6 cells that were used as the positive controls (Figure 4A and 4B). Similarly, immortalized NAF10 cells stably overexpressing CXCL14 were observed to be activated (Figure 4A). Moreover, CXCL14 treatment had an activating effect on NAF6 cells similar to that of CXCL12, but the effect was weaker than the effect observed after TGF-β treatment (Supplemental Figure 3A). Both CXCL12 and TGF-β are usually considered to be activators of mammary fibroblasts. In contrast, the addition of a neutralizing antibody to CXCL14 (αCXCL14) to the co-culture system containing NAF6 cells and HIC1-deleted MCF7/T47D cells significantly suppressed the activation of NAF6 cells compared with the respective controls (Figure 4C). These results indicate that CXCL14 originating from HIC1-deleted BrCa cells plays a critical role in inducing the activation of mammary gland fibroblasts.

Next, to investigate the effect of the HIC1/CXCL14 axis on BrCa progression in vivo, three MCF7 cell lines (Ctrl-NC, sgHIC1-NC, and sgHIC1-shCXCL14) were injected bilaterally into the fourth mammary fat pads of female BALB/c nude mice (Supplemental Figure 3B). Figures 4D and 4E show that both the volumes and the weights of the resulting tumors were greatly increased in the $MCF7^{sgHIC1\text{-}NC}$ group compared with the control $MCF7^{Ctrl\text{-}NC}$ group. However, knockdown of CXCL14 expression in $MCF7^{sgHIC1}$ cells markedly rescued the HIC1 deletion-induced tumor burden compared with $MCF7^{sgHIC1\text{-}NC}$ cells. Moreover, IHC staining indicated that Ki67 and stromal α-SMA expression was greatly increased in $MCF7^{sgHIC1\text{-}NC}$ xenografts compared with the controls, whereas knockdown of CXCL14 expression in $MCF7^{sgHIC1}$ cells markedly decreased the effects. These results were further confirmed by quantitative analysis (Figure 4F). Finally, using two Oncomine datasets, we found that the *CXCL14* mRNA levels were higher in BrCa tissues (n = 93) than they were in normal breast tissues (n = 9) (Supplemental Figure 3C). Altogether, these data suggest that CXCL14 derived from HIC1-deleted BrCa cells mediates the activation of mammary fibroblasts and that this activation is responsible for BrCa progression.

GPR85 is a novel functional receptor for CXCL14 activities

Based on our in vitro and in vivo findings, we next explored the mechanism through which CXCL14 mediates the activation of mammary fibroblasts. Supplemental Figure 4A shows that the ERK1/2 and Akt/p70 S6K

pathways were significantly activated after rhCXCL14 treatment of NAF6 and NAF7 cells. CAF6 and CAF7 cells were used as positive controls here. The ERK1/2 and Akt pathways were also activated in NAF6 cells when the cells were co-cultured with HIC1-deleted T47D cells (Supplemental Figure 4B). In contrast, the addition of αCXCL14 to the co-culture system abolished the effect (Supplemental Figure 4B), suggesting that the two pathways are potentially involved in the CXCL14-induced activation of mammary fibroblasts. To assess this possibility, two small-molecule inhibitors, U0126 (a MEK1/2 inhibitor) and LY294002 (a PI3K inhibitor), were used (Supplemental Figure 4C). Indeed, as shown in Supplemental Figures 4D-E and Supplemental Figures 5D, both U0126 and LY294002 obviously inhibited the expression of CAF markers not only in rhCXCL14-treated NAF6/NAF8/NAF10 cells but also in CAF10 cells, followed by inactivating the ERK1/2 and Akt pathways.

Previous studies have noted that the neddylation pathway, a newly characterized posttranslational modification pathway, is activated in both lung and liver cancers (29, 30). We therefore explored whether this pathway is associated with the activation of mammary fibroblasts. Supplemental Figure 5A shows that the entire neddylation pathway was activated in CAF6/8 cells compared with the activity of the pathway in the respective NAFs. A slight activation of the neddylation pathway was also observed in NAF6 and NAF10 cells after treatment with rhCXCL14 for 4 days (Supplemental Figure 5B). Furthermore, when primary CAF10 or CXCL14-activated NAF10 cells were treated with the neddylation inhibitor MLN4924, expression of the CAF markers was markedly reduced as determined by both Western blot and immunofluorescence assay (Supplemental Figures 5C and 5D). These results suggest that the neddylation pathway is also involved in the activation of mammary fibroblasts. Taken together, the results presented here demonstrate that CXCL14 secreted by HIC1-deleted BrCa cells activates mammary fibroblasts through the ERK1/2, Akt, and neddylation pathways.

Given that the receptor of CXCL14 has not yet been identified, primary NAF6 cells were treated with biotin-CXCL14 to determine its potential receptor. Immunofluorescence assay showed that CXCL14 was localized on the cell membrane (Figure 5A), suggesting that a receptor on the fibroblast surface may mediate the biological effects of CXCL14. Next, HuProt™ human proteome microarrays containing 18,583 affinity-purified N-terminally GST-tagged proteins were used to identify CXCL14-binding proteins (Figure 5B). Notably, approximately 3.1% of the proteins on the microarrays, including 32 membrane proteins, were found to bind CXCL14 (Supplemental Figures 6A-C). Ultimately, we focused on 2 known G protein-coupled receptors and 5 transmembrane receptors (JMJD6, ROBO3, KLRC1, TNFRSF10C, F2R, SLAMF6 and GPR85) (Figure 5C and Supplemental Figures 6D-E). Finally, as shown in Figure 5D, the orphan G protein-coupled receptor GPR85 (also called super conserved receptor expressed in brain 2, SREB2) was selected and subsequently confirmed to bind to CXCL14 in NAF6 cells using streptavidin-agarose pulldown assays. RNAi-

mediated silencing of GPR85 in NAF6 cells and its overexpression in 293T cells were performed to assay whether GPR85 is the functional receptor for CXCL14 (Supplemental Figures 6F and 6G). Being the accepted method for evaluating chemokine receptor activation (31), the calcium mobilization assay was used to measure changes in intracellular calcium ($[Ca^{2+}]_i$) upon CXCL14 stimulation. Figure 5E shows that NAF6 cells transfected with control siRNA (NC) responded to stimulation by both rhCXCL14 and rhCXCL12, whereas NAF6 cells transfected with GPR85-3 siRNA did not respond to rhCXCL14 but did respond to the positive control rhCXCL12. To evaluate the ability of CXCL14 to bind to GPR85, radioligand binding assays were next performed. Figure 5F shows that levels of specific binding for ^{125}I-CXCL14 were markedly higher in 293T-GPR85 cells than 293T-NC cells. Moreover, the high level of specific binding for ^{125}I-CXCL14 in GPR85 transfectants could be competed by unlabeled CXCL14 (IC50 = 0.436 nM, 0.0851-1.976 nM, 95% confidence interval; Figure 5G). Unlabeled CXCL12 and CXCL3 with the highest sequence homology of CXCL14 among the CXC chemokine family, show approximately 30% identity of amino acids and 55% similarity to CXCL14 when conservative changes are taken into account (32), also competed for ^{125}I-CXCL14 binding with much less affinity (IC50 = 2.338 nM for CXCL12, and IC50 = 4.568 nM for CXCL3; Figure 5G). Next, Western blot analysis demonstrated that rhCXCL14 markedly activated the Akt and ERK1/2 pathways in NAF6-NC cells but not in NAF6-siGPR85 cells, whereas activation of these signaling pathways was still observed in NAF6-siKLRC1 cells (Figure 5H and Supplemental Figure 6I). Notably, rhCXCL12 activated both the Akt and ERK1/2 pathways when GPR85 expression was reduced in NAF6 cells (Supplemental Figure 6H), suggesting that activation of the Akt and ERK1/2 pathways in NAFs by CXCL14 depends on GPR85. Next, we assayed the ability of CXCL14 to induce the activation of mammary fibroblasts after silencing of GPR85 expression. Figure 5I shows that inhibition of GPR85 expression in NAF6 cells followed by treatment with increasing concentrations of rhCXCL14 for 4 days attenuated the activation of expression of CAF markers compared with the effects observed in NAF6-NC cells. Similar effects were also noted in NAF6 cells co-cultured with HIC1-deleted MCF7 cells; the BrCa cells had a stronger activating effect on NAF6-NC cells than on NAF6-siGPR85 cells (Figure 5J). Notably, knockdown of GPR85 expression in CAF6 cells inhibited CAF marker expression and Akt, ERK1/2 signaling (Supplemental Figure 6K). Besides, Western blot assays suggested that CXCL14-induced degradation of GPR85 occurs in NAF6 cells, whereas this effect was not observed after rhCXCL12 treatment (Supplemental Figure 6J). Taken together, these findings indicate that the effects of chemokine CXCL14 on the activation of mammary fibroblasts are dependent on GPR85, a novel functional receptor for CXCL14.

To investigate whether GPR85 on NAFs could affect the growth and metastasis of BrCa in vivo, MDA-231-LM2 cells mixed with NAF13-NC or NAF13-shGPR85-3 cells at a ratio of 3:1 were injected unilaterally into the fourth mammary fat pads of female BALB/c nude mice (Supplemental Figure 7A). Supplemental

Figures 7B and 7C show that both volumes and weights of the tumors were greatly decreased in the NAF13-shGPR85-3 group compared with the control NAF13-NC group. Moreover, bioluminescence imaging of the harvested lungs demonstrated that lung metastasis was also markedly suppressed in the NAF13-shGPR85-3 group compared with the control group (Supplemental Figure 7D), which was further confirmed using human cytokeratin staining of lung sections to assess human cancer cell metastasis (Supplemental Figure 7E). Collectively, these data suggest that GPR85 on NAFs significantly affects the growth and lung metastasis of TNBC xenografts. One possible explanation is that GPR85-deficient NAFs could not be activated by CXCL14 secreted from the TNBC cells. Therefore, the data suggest that CXCL14/GPR85 axis is associated with growth and metastasis of TNBC.

Next, using IHC staining, we assayed the stromal p-ERK, p-Akt (Ser 473) and NEDD8 expression in orthotopic MCF7 xenografts as described in Figure 4E and MDA-231-LM2+NAF13 xenografts as described in Supplemental Figure 7A. The staining reveals that the levels of stromal p-ERK, p-Akt (Ser 473) and NEDD8 were markedly increased in $MCF7^{sgHIC1\text{-}NC}$ xenografts compared with the respective controls, whereas knockdown of CXCL14 expression in $MCF7^{sgHIC1}$ cells decreased these effects (Supplemental Figure 8A). Notable, these signaling pathways were similarly suppressed in the NAF13-shGPR85-3 group compared with the control NAF13-NC group (Supplemental Figure 8B), which were further confirmed by quantitative analysis (Supplemental Figure 8). In summary, the activation of stromal ERK, Akt and neddylation pathways were suppressed in vivo either by inhibiting CXCL14 secretion in BrCa cells or by reducing GPR85 expression on NAFs cells, indicating that the CXCL14/GPR85 axis is vital for activation of these signaling pathways.

CXCL14-activated fibroblasts induce migration of BrCa cells via CCL17

It has been reported that CAFs induce the migration of cancer cells by secreting cytokine-like molecules (6, 14). Here, we found that CXCL14-activated NAF10 cells enhanced the migration of MDA-231-LM2 BrCa cells, similar to the function of primary CAF10 cells (Figure 6A). Next, we explored whether cytokines secreted by the CXCL14-activated fibroblasts are responsible for modulating the migration of BrCa cells. Cytokine arrays were used to detect the secreted soluble factors derived from conditioned medium (CM) of NAF10, CXCL14-activated NAF10, and CAF10 cells (Figure 6B). Fig. 6B shows that the levels of CCL17, IL-5 and angiopoietin-2 were significantly increased in the CM of both CXCL14-activated NAF10 and CAF10 cells compared with the levels of these cytokines in the CM of NAF10 cells, suggesting that the cells may have similar phenotypes. Next, to assay the effects of these factors on BrCa cells, we used Boyden chambers in which MDA-231-LM2 cells were plated in the upper chambers and recombinant human CCL17, IL-5 or angiopoietin-2 were placed in the lower wells. The results showed that only CCL17 enhanced the migration of BrCa cells; the other two cytokines had no effect (Figure 6C). Consistent with the results obtained using

cytokine arrays, ELISA showed that CCL17 was secreted at high levels into the CM of CXCL14-activated NAF10 and CAF10 cells (Supplemental Figure 9A). However, the increased secretion of CCL17 was not markedly observed in NAF13 cells using RNAi-mediated silencing of GPR85 compared with the control cells after rhCXCL14 treatment. (Supplemental Figure 9B). As shown in Figure 6D, the addition of a neutralizing antibody to CCL17 (αCCL17) to the co-culture system dramatically suppressed the migration of BrCa cells compared with their respective controls. Furthermore, EMT phenotypes were observed in MCF7 and MDA-231-LM2 cells after treatment with increasing concentrations of rhCCL17 for 4 days, as indicated by decreased E-cadherin expression, increased N-cadherin expression and markedly increased migration and invasion abilities (Figure 6E and Supplemental Figures 9C-E). Similarly, the migration abilities of MDA-MB-231 cells and breast epithelial cell MCF 10A cells were markedly enhanced by rhCCL17 treatment compared with the respective controls (Supplemental Figure 9F). These results confirm that CCL17 originating from CXCL14-activated fibroblasts that display phenotypes similar to CAFs can facilitate the migration of BrCa cells and is potentially associated with EMT.

It was recently shown that CCR4, as the receptor for CCL17, can induce the migration of hepatocellular carcinoma cells via the Akt signaling pathway (33). Our mechanistic analyses revealed that CCL17 also activates the Akt/GSK-3β pathways through its receptor, CCR4, in both MCF7 and MDA-231-LM2 cells (Figures 6F and 6G). Moreover, RNAi-mediated silencing of CCR4 in these cells markedly inhibited the development of the CCL17-induced EMT phenotype and the activation of Akt signaling (Supplemental Figure 9G and Figure 6G), suggesting that the CCL17/CCR4 axis enhances EMT in BrCa cells through activation of the Akt/GSK-3β pathways.

Finally, we observed that rhCCL17 greatly induced EMT of HIC1-deleted MCF7 BrCa cells, whereas it had little effect on the control cells, suggesting that HIC1 deletion in BrCa cells markedly increases their sensitivity to CCL17-induced EMT (Supplemental Figure 9H).

CCL17 secreted by CAFs promotes lung metastasis of BrCa xenografts

Based on the above observations, we next assayed the effect of CCL17 secreted by CAFs on BrCa metastasis in vivo. MDA-231-LM2 cells mixed with primary NAF8 or CAF8 cells were injected bilaterally into the fourth mammary fat pads of female BALB/c nude mice. Two weeks later, when the xenografts became palpable, control IgG or a neutralizing antibody against CCL17 (αCCL17) was injected into the mice via the tail vein every 3 days. The treatment was maintained for 30 days, and the mice were then euthanized (Figure 7A and Supplemental Figure 10A). As shown in Figure 7B, bioluminescence imaging of the harvested lungs demonstrated that lung metastasis was markedly promoted in the CAF8+IgG group compared with the NAF8+IgG group. However, lung metastasis was greatly suppressed in the CAF8+αCCL17 group compared

with the CAF8+IgG group (Figure 7B), and this was further confirmed using human cytokeratin staining of lung sections to assess human cancer cell metastasis (Figure 7C). Furthermore, the expression of N-cadherin and vimentin was markedly increased in the orthotopic xenografts in the CAF8+IgG group compared with those in the NAF8+IgG group; however, the expression of both proteins was greatly reduced in the CAF8+αCCL17 group (Figure 7C). Notably, Kaplan-Meier analysis also indicated that αCCL17 treatment greatly increased the survival of the mice xenografted with MDA-231-LM2 cells mixed with CAF8 cells compared with IgG treatment (Figure 7D). Collectively, these data suggest that CCL17 secreted by CAFs promotes the lung metastasis of BrCa xenografts.

Finally, we observed that the stromal CCL17 mRNA levels were higher in BrCa tissues (n = 53) than in normal breast tissues (n = 6) in an Oncomine dataset (Finak Breast) (Supplemental Figure 10B). Using the TCGA database, we also noted that total CCL17 mRNA levels were significantly higher in 133 BrCa tissues than in paired normal tissues (Supplemental Figure 10C). Furthermore, CCL17 expression was significantly increased in 123 high-metastatic TNBC tissues compared with low-metastatic luminal BrCa tissues (Supplemental Figure 10C). Using the Kaplan-Meier method followed by the log-rank test, we further confirmed that higher expression of CCL17 correlated with lower distant metastasis-free survival in 543 systemically untreated patients (Figure 7E), whereas this correlation was not observed in all cases or systemically treated patients (data not shown) (27). These data imply that CCL17 expression is associated with poor prognosis of BrCa.

The HIC1-CXCL14-CCL17 loop is associated with malignant progression in BrCa patients

To determine whether our findings are clinically relevant, high-density tissue microarrays (TMA) containing 228 benign and malignant cases from BrCa patients were used to examine the expression of epithelial HIC1, stromal CXCL14, stromal CCL17, stromal GPR85 and epithelial CCR4 (Supplemental Figure 11A). As shown in Figure 8A and Supplemental Figure 11B, there were fewer cases with high expression of epithelial nuclear HIC1 among malignant BrCa patients than they were among benign patients. Notably, HIC1 expression was significantly associated with TNBC (P = 0.007 *vs* benign), which has the worst clinical prognosis among all breast cancer subtypes (Figure 8A and Supplemental Table 1). In particular, the expression of epithelial nuclear HIC1 correlated strongly with ER and PR expression (P < 0.001 and P = 0.001, respectively) (Supplemental Table 1). In contrast to HIC1, more cases with high expression of stromal CXCL14, stromal CCL17, stromal GPR85 and epithelial CCR4 were found among patients with malignant BrCa than in patients with benign diseases (Figure 8A; Supplemental Figures 11B and 11C). Interestingly, the expression of stromal CXCL14 was also markedly correlated with TNBC subtype and ER/PR expression (P = 0.017 *vs* benign, P = 0.001 and P < 0.001, respectively) (Figure 8A and Supplemental Figure 11B).

Expression of stromal GPR85 was significantly lower in benign/Luminal patients than HER2+/TNBC patients (Supplemental Figures 11B and 11C). Furthermore, the stromal CCL17 and epithelial CCR4 levels were higher in all three BrCa subtypes than benign patients, but there was no significant difference among the three subtypes (Figure 8A; Supplemental Figures 11B, 11C; Supplemental Table 1). Besides, the mRNA expression of stromal GPR85 and total CCR4 was all observed to be up-regulated in BrCa tissues compared with normal tissues in two Oncomine datasets and TCGA database (Supplemental Figures 11D and 11E). Thus, HIC1 and CXCL14/GPR85/CCL17/CCR4 expression are potential prognostic factors associated with poor prognosis of BrCa.

Finally, we found that the cases that had high epithelial nuclear HIC1 levels often displayed low stromal CXCL14 or CCL17 expression and vice versa (Figure 8B). Spearman's rank correlation coefficient analysis was performed to determine whether the observed differences in expression of the three proteins had statistical significance (Table 1). Indeed, there was an inverse correlation between epithelial HIC1 and stromal CXCL14 levels and a positive correlation between stromal CXCL14 and CCL17 levels (Table 1). Moreover, *CXCL14* expression tended to be positively associated with the expression of *CCL17* in Basal-like BrCa in the TCGA database (Supplemental Figure 11F). Collectively, especially with respect to the potential prognostic markers for the TNBC subtype, these data suggest that the HIC1-CXCL14-CCL17 loop is associated with malignant progression in BrCa patients.

Discussion

The tumor suppressor gene *HIC1* has been widely documented to play a vital role in the process of BrCa development (21, 25, 34, 35). However, the use of mice with a conditional knockout of HIC1 in the mammary gland to assay the specific function of the *HIC1* gene in BrCa in vivo has not yet been reported. Here, we showed that conditional deletion of HIC1 in the mouse mammary gland may contribute to premalignant transformation at the early stage of tumor formation, inducing the formation of hyperplastic epithelium and increased expression of the proliferative markers Ki67/cyclin D1 in mammary gland. Mechanistically, loss of HIC1 expression in lung cancer contributes to malignant transformation through the acquisition of chromosomal instability (36), which suggests that it may also correlate with mammary gland tumorigenesis. Furthermore, it has been reported that HIC1 acts as a nuclear modulator of the Wnt signaling pathway by recruiting TCF-4 and β-catenin to HIC1 bodies to exert its suppression functions (37). Indeed, we found that overexpression of HIC1 could repress stemness of BrCa cells in vitro (data not shown). In addition, lactogenic defects of mammary glands were also observed in *Hic1*$^{-/-}$ mice; this defect may be associated with Wnt signaling, which plays a significant role in the self-renewal of mammary stem cells and in mammary gland development (38-40).

It has been reported that BrCa cells and mammary fibroblasts cooperate and depend upon each other to promote the development of primary tumors to aggressive disease (41). In the work reported in this manuscript, we found that chemokine CXCL14 secreted by HIC1-deleted BrCa cells induces a functional conversion of NAFs to CAFs; in turn, the activated CAFs could promote metastasis of BrCa cells through secretion of the chemokine CCL17 (Figure 8C). Moreover, using breast tissue microarrays, we confirmed that the HIC1-CXCL14-CCL17 loop is associated with malignant progression in BrCa patients.

Chemokine (C-X-C motif) ligand 14 (CXCL14), a small cytokine belonging to the CXC chemokine family that is also known as BRAK (for breast and kidney-expressed chemokine). CXCL14 is responsible for the broad chemotactic activity in activated NK cells, dendritic cells, monocytes and macrophages (42-44). However, the effect of CXCL14 on cancer development remains controversial. Some reports have claimed antitumor and antiangiogenic effects of CXCL14 (45, 46), whereas others noted upregulated expression of CXCL14 in several cancer types, including BrCa and osteosarcoma (47, 48). A recent study also showed that CXCL14 expression in high stromal tissue but not in epithelial tissue is significantly associated with shorter survival in BrCa patients (49), raising the possibility that stromal CXCL14 may exert a pro-cancer role in BrCa progression (50). Moreover, a general association between the activation of mesenchymal cells and CXCL14 has been reported in that CXCL14 is upregulated in activated hepatic stellate cells, which are the main source of extracellular matrix and myofibroblast production (51). Here, we found that CXCL14 has the

novel role of activating mammary fibroblasts. It is well known that chemokines exert their effects by binding to specific transmembrane receptors, most of which are members of the seven-transmembrane, G protein-coupled receptor family (GPCRs). Notably, the cognate receptor for chemokine CXCL14 has still not been definitively identified. In fact, the induction of calcium influx by CXCL14 in PGE-treated monocytes has been observed, suggesting that a GPCR may be involved in CXCL14 signal transduction (42). In this regard, using HuProt™ human proteome microarrays, we found that CXCL14 specifically binds to GPR85 on the cellular membrane of NAFs to exert its biological effects. GPR85, also known as SREB2, is a member of the highly conserved SREB receptor family. It is one of the orphan receptors which is the most evolutionarily conserved GPCR and shares 100% amino acid sequence identity in a number of species, including humans and mice (52). GPR85 has been reported to express virtually in all neurons but most abundantly in hippocampal dentate gyrus and subventricular zone of the amygdala (53). Interestingly, CXCL14 is also considered to be a primordial or ancient CXC chemokine based on sequence conservation among species and their homeostatic roles (54), which mediated functions within the developing central nervous system (CNS) included chemotaxis of neurons. Although the receptor for CXCL14 is as yet reported, but because conserved ligands tend to bind to conserved receptors (55), the receptor for CXCL14 is probably also conserved. So far, there is no article reporting the function or expression of GPR85 in any other tissues except CNS. Here, expression of GPR85 protein in a variety of cells were observed, indicating that GPR85 levels in stromal cells (NAF/CAF13, Treg and macrophage) were higher than other cells (such as 293T, MCF7, Neuro-2A and THP-1 cells, data not shown), which suggest that GPR85 may play a vital role in microenvironment of BrCa. Furthermore, mechanistic analyses showed that the CXCL14/GPR85 chemokine axis is responsible for activating mammary fibroblasts through the ERK1/2, Akt, and neddylation pathways. Nevertheless, these pathways were found to be independent of each other in their activation of stromal fibroblasts (data not shown).

Finally, we showed that both CAFs and CXCXL14-activated NAFs can induce migration in vitro and metastasis in vivo of BrCa cells by secreting the potential chemokine CCL17. C-C chemokine ligand 17 (CCL17), originally known as thymus and activation-regulated chemokine (TARC), was shown to be expressed constitutively in thymus tissue and transiently in stimulated peripheral blood mononuclear cells (56). This chemokine is reported to specifically bind to and induce chemotaxis in T cells and to exert its effects by interacting with the chemokine receptor CCR4 (56, 57). CCR4 is a key receptor in the regulation of chemokine-dependent immune homeostasis and is selectively expressed by regulatory T cells and Th2 cells. Recent studies have shown that colon and breast cancer cells also express functional CCR4 receptors (58, 59) and that these receptors trigger remote induction of CCL17 in the lungs of mice and mediate CCR4-dependent pulmonary metastasis of BrCa cells (60). Among the stromal cells in the tumor microenvironment, tumor-associated macrophages have been reported to promote the process of EMT in hepatocellular carcinoma cells

through the secretion of CCL17 (61). However, the role of the CCL17 secreted by CAFs in BrCa development is still unclear. Our data show that activated CAFs promote the migration of cancer cells in vitro and the metastasis of BrCa in vivo through the CCL17/CCR4 axis upon activation of the Akt/GSK-3β signaling pathway.

Notably, we found that HIC1-deleted BrCa cells display increased sensitivity to the induction of EMT by CCL17 compared to the respective control cells, suggesting that the crosstalk between HIC1-deleted BrCa cells and mammary fibroblasts is vital for BrCa development.

In conclusion, we find that the HIC1-CXCL14-CCL17-CCR4 loop is essential for BrCa progression. The activation of this loop in BrCa tissue may serve as a potential prognostic marker and may provide the basis for more effective treatment strategies.

Methods

Cell culture

MDA-MB-231, MCF7, T47D human breast cancer cells, MCF 10A human breast epithelial cells and 293T embryonic kidney cells were obtained from American Type Culture Collection (ATCC) and grown according to standard protocols. MDA-231-LM2 human breast cancer cells were kindly provided and cultured as recommended by professor J. Massague (Memorial Sloan-Kettering Cancer Center). Primary mammary fibroblasts were isolated from 13 cases of freshly removed BrCa patients, and additional details are described in the Supplemental data. The cell lines were tested and authenticated by DNA typing in Shanghai Jiao Tong University Analysis Core and were cultured in a 37 °C water-saturated 5% CO_2 atmosphere.

Mice

The *Wap-Cre* transgenic mice with a C57BL/6 background were initially generated by Shanghai Biomodel Organism Science & Technology Development (SBOSTD) Co., Ltd. The *Hic1*$^{flox/flox}$ transgenic mice with a C57BL/6 background were kindly provided by Dr. Vladimir Korinek (Institute of Molecular Genetics, Academy of Sciences of the Czech Republic, Prague, Czech Republic) (62). All mice were kept under specific pathogen-free (SPF) conditions. To ameliorate any suffering of mice observed throughout these experimental studies, mice were euthanized by CO_2 inhalation. The protocol is in accordance with the Animal Welfare Policy of Shanghai Jiao Tong University School of Medicine and approved by School of Medicine IACUC, the IACUC protocol number is A-2016-015.

Generation of conditional knockout mice

A Cre-mediated specific *HIC1* gene deletion in luminal mammary epithelial cells was achieved by crossing *Hic1*$^{flox/flox}$ mice with *Wap-Cre* mice to produce *Hic1*$^{flox/+}$/*Wap-Cre*$^{+}$ mice. Double heterozygous *Hic1*$^{flox/+}$/ *Wap-Cre*$^{+}$ mice were then crossed with *Hic1*$^{flox/flox}$ mice to produce *Hic1*$^{flox/flox}$/*Wap-Cre*$^{+}$ mice. Next, *Hic1*$^{flox/flox}$/*Wap-Cre*$^{+}$ mice were bred with *Hic1*$^{flox/flox}$ mice to produce offspring that were used in our experiments. The *Hic1*$^{flox/flox}$ mice were used as the *Hic1*$^{+/+}$ controls, and the *Hic1*$^{flox/flox}$/*Wap-Cre*$^{+}$ mice were used as the *Hic1*$^{-/-}$ group. To avoid problems in nursing pups that were caused by mothers with potentially defective mammary glands, only the male mice of the breeding pairs carried the *Cre* transgene. The genotypes of the offspring were determined by PCR amplification of DNA obtained from the tails of the animals. Primers for PCR-based genotyping are listed in the Supplemental Data.

Luciferase reporter assays and chromatin immunoprecipitation (ChIP)

The *CXCL14* promoters and its truncated constructs were generated from genomic DNA of the human breast epithelial cell line MCF10A. All constructs and their mutants were inserted into the pGL3-Basic reporter gene vector. ChIP was performed according to published protocols, with slight modifications (26). Additional details are provided in the Supplemental data.

Cytokine arrays

Cytokine arrays (Proteome Profiler™ Human XL Cytokine Array Kit, Cat. no. c8052; R&D Systems) were used to survey the changes in 102 cytokines and chemokines in CM obtained from NAF10, CXCL14-activated NAF10 and CAF10 cells. NAF10 cells were treated with 100 ng/ml rhCXCL14 for 4 days, then seeded into 6-well plates containing unprocessed NAF10 and CAF10 cells. After 48 h, the cell culture supernatants were collected and incubated overnight with the array. Next, the membranes were washed to remove unbound materials and incubated with a cocktail of biotinylated antibodies. Streptavidin-HRP and chemiluminescent detection reagents were then applied, and a signal was produced at each capture spot corresponding to the amount of protein bound. The membranes were exposed to X-ray film for 10 minutes, and profiles of the mean spot pixel densities were analyzed using Protein Array Analyzer for ImageJ.

Tumor xenografts

To establish orthotopic BrCa xenografts, 5×10^6 MCF7 cells ($MCF7^{NC\text{-}NC}$, $MCF7^{sgHIC1\text{-}NC}$, $MCF7^{sgHIC1\text{-}shCXCL14}$) were injected bilaterally into the fourth mammary fat pads of female BALB/c nude mice (n = 10 per group). To supplement estrogen for MCF7 growth, each mouse was implanted with a pellet containing 0.72 mg of 17β-estradiol (Cat. no. NE-121; Innovative Research) 3 days prior to MCF7 injection. Tumor growth was evaluated by monitoring tumor volume with calipers (length × width^2 × 0.5) every 5 days. The animals were euthanized 6 weeks later, and the tumor xenografts were harvested for further investigation.

To establish orthotopic lung metastatic mouse models of MDA-231-LM2 BrCa cells, 1×10^6 MDA-231-LM2 cells mixed with primary NAFs or CAFs cells at a ratio of 3:1 were orthotopically implanted into the mammary fat pads of BALB/c nude mice. When the xenografts were palpable (approximately 0.5 cm in diameter), tail vein injection of control IgG or a neutralizing antibody against CCL17 (Cat. no. MAB364; R&D Systems) (1 μg/mouse) was performed every 3 days for 4 weeks. The lungs of the animals bearing breast tumor xenografts that stably express luciferase were analyzed using the Xenogen IVIS Imaging System.

Tissue microarrays (TMA)

High-density tissue microarrays (TMA) of human BrCa clinical samples (Cat. no. BRC2281) were obtained from a cohort of 228 patients and constructed by Superbiotek Inc. (Shanghai, China). The use of the clinical samples in the project was approved by the Shanghai Jiao Tong University School of Medicine Ethical Committee. IHC staining was performed with specific antibodies against HIC1 (Cat. no. bs15485R; Bioss), CXCL14 (Cat. no. ab46010; Abcam), CCL17 (Cat. no. ab195044; Abcam), GPR85 (Cat. no. ab140783; Abcam) and CCR4 (Cat. no. ab1669; Abcam). Additional details are provided in the Supplemental Data.

Statistics

All statistical analyses were performed using SPSS for Windows version 13.0 (SPSS). Two-tailed Student's t tests were used for comparisons between two groups, and one-way ANOVA followed by Bonferroni's post-

hoc test was used for multiple comparisons (three or more groups). The Kaplan-Meier curves for survival analyses were determined using the log-rank test. For multiple group comparisons and repeated measures of in vivo data, repeated-measures ANOVA (RM ANOVA) followed by a post-hoc LSD test were performed. Chi-square tests were applied to analyze the relationship between protein levels and clinicopathological status in BrCa tissue microarrays. Spearman's rank correlation coefficient analysis was performed to assess the relationship among epithelial HIC1, stromal CXCL14 and CCL17 in the BrCa tissue microarrays, as well as the correlation of *CXCL14* expression with *CCL17* expression in TCGA database. All experiments for cell cultures were performed independently at least three times and in triplicate each time. In all cases, P values < 0.05 were considered statistically significant.

Study approval

All murine studies were conducted under the approved Shanghai Jiao Tong University School of Medicine IACUC, the IACUC protocol number is A-2016-015. For all human studies, written informed consent was received from participants prior to inclusion in the study where required. All samples were obtained in accordance with standard protocols of the Renji Hospital Ethics Committee of Shanghai Jiao Tong University School of Medicine.

Author contributions

JW, YW, ZH, JL and XM conceived and designed the study. YW, XW and LW acquired the data. YW and LW analyzed the data. YJ and JL provided resources. MH, YL, LH, YL, TW, MY, GL and GF supervised the study. YW and JW wrote and reviewed the manuscript.

Acknowledgements

It is appreciated for comments from Prof. Ceshi Chen and Binhua Zhou. Research in the authors' laboratory is supported by the National Natural Funding of China (81272404, 81772806, 81702535), National key program (973) for Basic Research of China (2011CB510106), the Program for Professor of Special Appointment (Eastern Scholar to J, Wang) at Shanghai Institutions of Higher Learning.

References

1. Siegel RL, Miller KD, and Jemal A. Cancer Statistics, 2017. *CA: a cancer journal for clinicians.* 2017;67(1):7-30.
2. DeSantis CE, Ma J, Goding Sauer A, Newman LA, and Jemal A. Breast cancer statistics, 2017, racial disparity in mortality by state. *CA: a cancer journal for clinicians.* 2017;67(6):439-48.
3. Paget S. The distribution of secondary growths in cancer of the breast. 1889. *Cancer metastasis reviews.* 1989;8(2):98-101.
4. Quail DF, and Joyce JA. Microenvironmental regulation of tumor progression and metastasis. *Nature medicine.* 2013;19(11):1423-37.
5. Ishii G, Ochiai A, and Neri S. Phenotypic and functional heterogeneity of cancer-associated fibroblast within the tumor microenvironment. *Adv Drug Deliv Rev.* 2016;99(Pt B):186-96.
6. Orimo A, Gupta PB, Sgroi DC, Arenzana-Seisdedos F, Delaunay T, Naeem R, et al. Stromal fibroblasts present in invasive human breast carcinomas promote tumor growth and angiogenesis through elevated SDF-1/CXCL12 secretion. *Cell.* 2005;121(3):335-48.
7. Dumont N, Liu B, DeFilippis RA, Chang H, Rabban JT, Karnezis AN, et al. Breast Fibroblasts Modulate Early Dissemination, Tumorigenesis, and Metastasis through Alteration of Extracellular Matrix Characteristics. *Neoplasia (New York, NY).* 2013;15(3):249-IN7.
8. Kojima Y, Acar A, Eaton EN, Mellody KT, Scheel C, Ben-Porath I, et al. Autocrine TGF-beta and stromal cell-derived factor-1 (SDF-1) signaling drives the evolution of tumor-promoting mammary stromal myofibroblasts. *Proceedings of the National Academy of Sciences of the United States of America.* 2010;107(46):20009-14.
9. Trimboli AJ, Cantemir-Stone CZ, Li F, Wallace JA, Merchant A, Creasap N, et al. Pten in stromal fibroblasts suppresses mammary epithelial tumours. *Nature.* 2009;461(7267):1084-91.
10. Procopio MG, Laszlo C, Al Labban D, Kim DE, Bordignon P, Jo SH, et al. Combined CSL and p53 downregulation promotes cancer-associated fibroblast activation. *Nature cell biology.* 2015;17(9):1193-204.
11. Hill R, Song Y, Cardiff RD, and Van Dyke T. Selective evolution of stromal mesenchyme with p53 loss in response to epithelial tumorigenesis. *Cell.* 2005;123(6):1001-11.
12. Trimis G, Chatzistamou I, Politi K, Kiaris H, and Papavassiliou AG. Expression of p21waf1/Cip1 in stromal fibroblasts of primary breast tumors. *Human molecular genetics.* 2008;17(22):3596-600.
13. Trimmer C, Sotgia F, Whitaker-Menezes D, Balliet RM, Eaton G, Martinez-Outschoorn UE, et al. Caveolin-1 and mitochondrial SOD2 (MnSOD) function as tumor suppressors in the stromal microenvironment. *Cancer biology & therapy.* 2014;11(4):383-94.
14. Studebaker AW, Storci G, Werbeck JL, Sansone P, Sasser AK, Tavolari S, et al. Fibroblasts isolated from common sites of breast cancer metastasis enhance cancer cell growth rates and invasiveness in an interleukin-6-dependent manner. *Cancer research.* 2008;68(21):9087-95.
15. Zheng J, Wang J, Sun X, Hao M, Ding T, Xiong D, et al. HIC1 modulates prostate cancer progression by epigenetic modification. *Clinical cancer research : an official journal of the American Association for Cancer Research.* 2013;19(6):1400-10.
16. Wang X, Wang Y, Xiao G, Wang J, Zu L, Hao M, et al. Hypermethylated in cancer 1(HIC1) suppresses non-small cell lung cancer progression by targeting interleukin-6/Stat3 pathway. *Oncotarget.* 2016;7(21):30350-64.
17. Fujii H, Biel MA, Zhou W, Weitzman SA, Baylin SB, and Gabrielson E. Methylation of the HIC-1 candidate tumor suppressor gene in human breast cancer. *Oncogene.* 1998;16(16):2159-64.
18. Wales MM, Biel MA, el Deiry W, Nelkin BD, Issa JP, Cavenee WK, et al. p53 activates expression of HIC-1, a new candidate tumour suppressor gene on 17p13.3. *Nature medicine.* 1995;1(6):570-7.
19. Chen WY, Wang DH, Yen RC, Luo J, Gu W, and Baylin SB. Tumor suppressor HIC1 directly regulates SIRT1 to modulate p53-dependent DNA-damage responses. *Cell.* 2005;123(3):437-48.
20. Pinte S, Stankovic-Valentin N, Deltour S, Rood BR, Guerardel C, and Leprince D. The tumor suppressor gene HIC1 (hypermethylated in cancer 1) is a sequence-specific transcriptional repressor: definition of its consensus binding sequence and analysis of its DNA binding and repressive properties. *The Journal of biological chemistry.* 2004;279(37):38313-24.

21. Cheng G, Sun X, Wang J, Xiao G, Wang X, Fan X, et al. HIC1 silencing in triple-negative breast cancer drives progression through misregulation of LCN2. *Cancer research.* 2014;74(3):862-72.
22. Carter MG, Johns MA, Zeng X, Zhou L, Zink MC, Mankowski JL, et al. Mice deficient in the candidate tumor suppressor gene Hic1 exhibit developmental defects of structures affected in the Miller-Dieker syndrome. *Human molecular genetics.* 2000;9(3):413-9.
23. Chen WY, Zeng X, Carter MG, Morrell CN, Chiu Yen RW, Esteller M, et al. Heterozygous disruption of Hic1 predisposes mice to a gender-dependent spectrum of malignant tumors. *Nature genetics.* 2003;33(2):197-202.
24. Van Rechem C, Rood BR, Touka M, Pinte S, Jenal M, Guerardel C, et al. Scavenger chemokine (CXC motif) receptor 7 (CXCR7) is a direct target gene of HIC1 (hypermethylated in cancer 1). *The Journal of biological chemistry.* 2009;284(31):20927-35.
25. Zhang W, Zeng X, Briggs KJ, Beaty R, Simons B, Chiu Yen RW, et al. A potential tumor suppressor role for Hic1 in breast cancer through transcriptional repression of ephrin-A1. *Oncogene.* 2010;29(17):2467-76.
26. Hao M, Li Y, Wang J, Qin J, Wang Y, Ding Y, et al. HIC1 loss promotes prostate cancer metastasis by triggering epithelial-mesenchymal transition. *The Journal of pathology.* 2017;242(4):409-20.
27. Gyorffy B, Lanczky A, Eklund AC, Denkert C, Budczies J, Li Q, et al. An online survival analysis tool to rapidly assess the effect of 22,277 genes on breast cancer prognosis using microarray data of 1,809 patients. *Breast cancer research and treatment.* 2010;123(3):725-31.
28. Loeffler M, Kruger JA, Niethammer AG, and Reisfeld RA. Targeting tumor-associated fibroblasts improves cancer chemotherapy by increasing intratumoral drug uptake. *The Journal of clinical investigation.* 2006;116(7):1955-62.
29. Li L, Wang M, Yu G, Chen P, Li H, Wei D, et al. Overactivated neddylation pathway as a therapeutic target in lung cancer. *Journal of the National Cancer Institute.* 2014;106(6).
30. Xu J, Li L, Yu G, Ying W, Gao Q, Zhang W, et al. The neddylation-cullin 2-RBX1 E3 ligase axis targets tumor suppressor RhoB for degradation in liver cancer. *Mol Cell Proteomics.* 2015;14(3):499-509.
31. Chen J, Yao Y, Gong C, Yu F, Su S, Chen J, et al. CCL18 from tumor-associated macrophages promotes breast cancer metastasis via PITPNM3. *Cancer Cell.* 2011;19(4):541-55.
32. Hromas R, Broxmeyer HE, Kim C, Nakshatri H, Christopherson K, 2nd, Azam M, et al. Cloning of BRAK, a novel divergent CXC chemokine preferentially expressed in normal versus malignant cells. *Biochemical and biophysical research communications.* 1999;255(3):703-6.
33. Cheng X, Wu H, Jin ZJ, Ma D, Yuen S, Jing XQ, et al. Up-regulation of chemokine receptor CCR4 is associated with Human Hepatocellular Carcinoma malignant behavior. *Scientific reports.* 2017;7(1):12362.
34. Wang Y, Liang H, Zhou G, Hu X, Liu Z, Jin F, et al. HIC1 and miR-23~27~24 clusters form a double-negative feedback loop in breast cancer. *Cell death and differentiation.* 2017;24(3):421-32.
35. Boulay G, Malaquin N, Loison I, Foveau B, Van Rechem C, Rood BR, et al. Loss of Hypermethylated in Cancer 1 (HIC1) in breast cancer cells contributes to stress-induced migration and invasion through beta-2 adrenergic receptor (ADRB2) misregulation. *The Journal of biological chemistry.* 2012;287(8):5379-89.
36. Szczepny A, Carey K, McKenzie L, Jayasekara WSN, Rossello F, Gonzalez-Rajal A, et al. The tumor suppressor Hic1 maintains chromosomal stability independent of Tp53. *Oncogene.* 2018;37(14):1939-48.
37. Valenta T, Lukas J, Doubravska L, Fafilek B, and Korinek V. HIC1 attenuates Wnt signaling by recruitment of TCF-4 and beta-catenin to the nuclear bodies. *The EMBO journal.* 2006;25(11):2326-37.
38. Boras-Granic K, and Hamel PA. Wnt-signalling in the embryonic mammary gland. *Journal of mammary gland biology and neoplasia.* 2013;18(2):155-63.
39. Turashvili G, Bouchal J, Burkadze G, and Kolar Z. Wnt signaling pathway in mammary gland development and carcinogenesis. *Pathobiology : journal of immunopathology, molecular and cellular biology.* 2006;73(5):213-23.
40. Zeng YA, and Nusse R. Wnt proteins are self-renewal factors for mammary stem cells and promote their long-term expansion in culture. *Cell stem cell.* 2010;6(6):568-77.
41. Avgustinova A, Iravani M, Robertson D, Fearns A, Gao Q, Klingbeil P, et al. Tumour cell-derived Wnt7a recruits and activates fibroblasts to promote tumour aggressiveness. *Nature communications.* 2016;7:10305.
42. Kurth I, Willimann K, Schaerli P, Hunziker T, Clark-Lewis I, and Moser B. Monocyte selectivity and tissue localization suggests a role for breast and kidney-expressed chemokine (BRAK) in macrophage development. *The Journal of*

experimental medicine. 2001;194(6):855-61.

43. Starnes T, Rasila KK, Robertson MJ, Brahmi Z, Dahl R, Christopherson K, et al. The chemokine CXCL14 (BRAK) stimulates activated NK cell migration: implications for the downregulation of CXCL14 in malignancy. *Experimental hematology.* 2006;34(8):1101-5.
44. Shurin GV, Ferris RL, Tourkova IL, Perez L, Lokshin A, Balkir L, et al. Loss of new chemokine CXCL14 in tumor tissue is associated with low infiltration by dendritic cells (DC), while restoration of human CXCL14 expression in tumor cells causes attraction of DC both in vitro and in vivo. *J Immunol.* 2005;174(9):5490-8.
45. Shellenberger TD, Wang M, Gujrati M, Jayakumar A, Strieter RM, Burdick MD, et al. BRAK/CXCL14 is a potent inhibitor of angiogenesis and a chemotactic factor for immature dendritic cells. *Cancer research.* 2004;64(22):8262-70.
46. Hata R, Izukuri K, Kato Y, Sasaki S, Mukaida N, Maehata Y, et al. Suppressed rate of carcinogenesis and decreases in tumour volume and lung metastasis in CXCL14/BRAK transgenic mice. *Scientific reports.* 2015;5:9083.
47. Allinen M, Beroukhim R, Cai L, Brennan C, Lahti-Domenici J, Huang H, et al. Molecular characterization of the tumor microenvironment in breast cancer. *Cancer Cell.* 2004;6(1):17-32.
48. Lu J, Song G, Tang Q, Zou C, Han F, Zhao Z, et al. IRX1 hypomethylation promotes osteosarcoma metastasis via induction of CXCL14/NF-kappaB signaling. *The Journal of clinical investigation.* 2015;125(5):1839-56.
49. Sjoberg E, Augsten M, Bergh J, Jirstrom K, and Ostman A. Expression of the chemokine CXCL14 in the tumour stroma is an independent marker of survival in breast cancer. *British journal of cancer.* 2016;114(10):1117-24.
50. Gu XL, Ou ZL, Lin FJ, Yang XL, Luo JM, Shen ZZ, et al. Expression of CXCL14 and its anticancer role in breast cancer. *Breast cancer research and treatment.* 2012;135(3):725-35.
51. De Minicis S, Seki E, Uchinami H, Kluwe J, Zhang Y, Brenner DA, et al. Gene expression profiles during hepatic stellate cell activation in culture and in vivo. *Gastroenterology.* 2007;132(5):1937-46.
52. Matsumoto M, Straub RE, Marenco S, Nicodemus KK, Matsumoto S, Fujikawa A, et al. The evolutionarily conserved G protein-coupled receptor SREB2/GPR85 influences brain size, behavior, and vulnerability to schizophrenia. *Proceedings of the National Academy of Sciences of the United States of America.* 2008;105(16):6133-8.
53. Matsumoto M, Beltaifa S, Weickert CS, Herman MM, Hyde TM, Saunders RC, et al. A conserved mRNA expression profile of SREB2 (GPR85) in adult human, monkey, and rat forebrain. *Brain Res Mol Brain Res.* 2005;138(1):58-69.
54. Huising MO, van der Meulen T, Flik G, and Verburg-van Kemenade BM. Three novel carp CXC chemokines are expressed early in ontogeny and at nonimmune sites. *Eur J Biochem.* 2004;271(20):4094-106.
55. Murphy PM. Molecular mimicry and the generation of host defense protein diversity. *Cell.* 1993;72(6):823-6.
56. Imai T, Yoshida T, Baba M, Nishimura M, Kakizaki M, and Yoshie O. Molecular cloning of a novel T cell-directed CC chemokine expressed in thymus by signal sequence trap using Epstein-Barr virus vector. *The Journal of biological chemistry.* 1996;271(35):21514-21.
57. Imai T, Baba M, Nishimura M, Kakizaki M, Takagi S, and Yoshie O. The T cell-directed CC chemokine TARC is a highly specific biological ligand for CC chemokine receptor 4. *The Journal of biological chemistry.* 1997;272(23):15036-42.
58. Li JY, Ou ZL, Yu SJ, Gu XL, Yang C, Chen AX, et al. The chemokine receptor CCR4 promotes tumor growth and lung metastasis in breast cancer. *Breast cancer research and treatment.* 2012;131(3):837-48.
59. Al-haidari AA, Syk I, Jirstrom K, and Thorlacius H. CCR4 mediates CCL17 (TARC)-induced migration of human colon cancer cells via RhoA/Rho-kinase signaling. *Int J Colorectal Dis.* 2013;28(11):1479-87.
60. Olkhanud PB, Baatar D, Bodogai M, Hakim F, Gress R, Anderson RL, et al. Breast cancer lung metastasis requires expression of chemokine receptor CCR4 and regulatory T cells. *Cancer research.* 2009;69(14):5996-6004.
61. Zhu F, Li X, Chen S, Zeng Q, Zhao Y, and Luo F. Tumor-associated macrophage or chemokine ligand CCL17 positively regulates the tumorigenesis of hepatocellular carcinoma. *Medical oncology.* 2016;33(2):17.
62. Pospichalova V, Tureckova J, Fafilek B, Vojtechova M, Krausova M, Lukas J, et al. Generation of two modified mouse alleles of the Hic1 tumor suppressor gene. *Genesis.* 2011;49(3):142-51.

Figures and figure legends

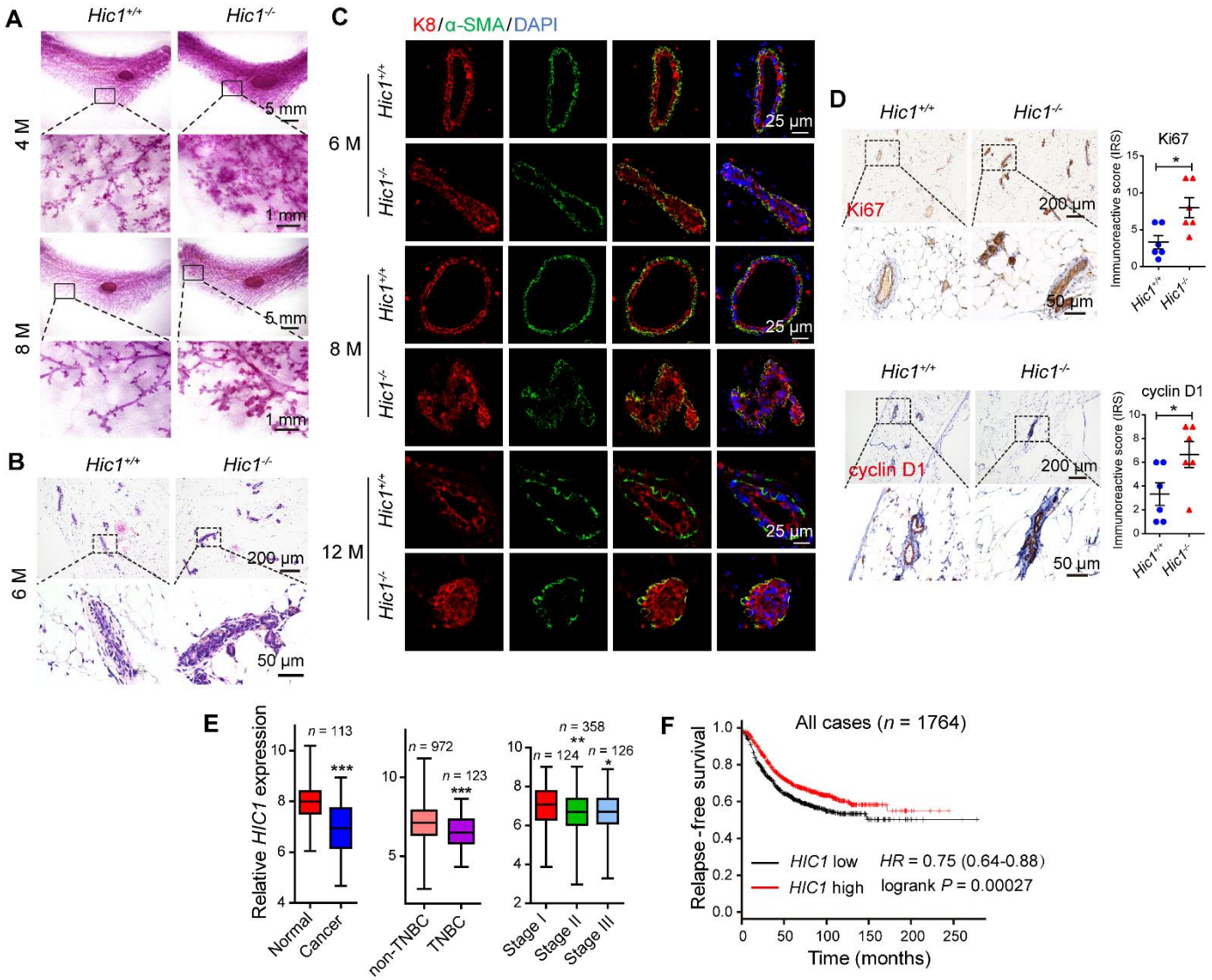

Figure 1. HIC1 deletion induces hyperplasia of mammary gland in vivo

(A) Representative whole-mount staining of the fourth inguinal mammary glands at the indicated ages (4 months (4 M) and 8 months (8 M)) were prepared from *Hic1*$^{+/+}$ mice or *Hic1*$^{-/-}$ mice and stained with carmine aluminum (n = 6 for each group). **(B)** H&E staining of the mammary glands of 6-month-old (6 M) mice. **(C)** Immunofluorescence staining of luminal epithelial marker (K8) and myoepithelial markers (α-SMA) in the mammary glands of 6 M, 8 M and 12 M mice. **(D)** Immunohistochemical staining of Ki67 and cyclin D1 in mammary glands of 6 M mice. The dot plots show the mean value for each immunoreactivity score (IRS) with statistical evaluation (mean ± SEM, n = 6; $^{*}P < 0.05$, P values were obtained using two-tailed Student's t tests). **(E)** Box plots of *HIC1* mRNA levels in paired normal breast/BrCa tissues (left, paired t tests), non-TNBC/TNBC tissues (middle, two-tailed Student's t tests) and BrCa tissues at different stages (right, one-way ANOVA followed by Bonferroni's post-hoc test). The data were obtained from the TCGA dataset (TCGA_BRCA_exp_HiSeqV2-2015-02-24). $^{*}P < 0.05$, $^{**}P < 0.01$ and $^{***}P < 0.001$. **(F)** Kaplan-Meier plots of the relapse-free survival (RFS) of patients with BrCa in whole datasets stratified by *HIC1* expression. The data were acquired from the Kaplan-Meier plotter database (P = 0.00027, P values were obtained using the

log-rank test) (27). The representative images in this figure were obtained from at least 3 animals of each genotype.

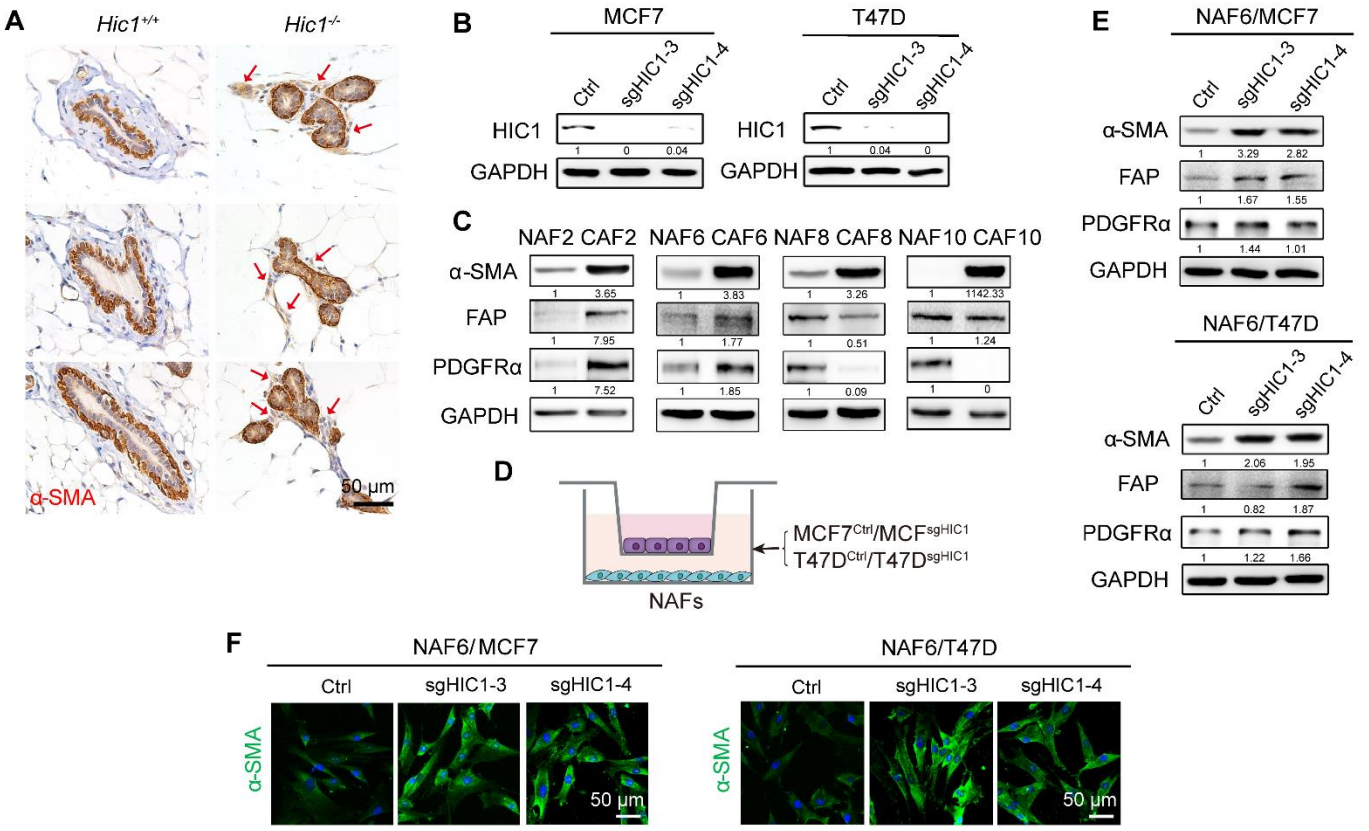

Figure 2. HIC1-deleted BrCa cells induce the activation of stromal fibroblasts in mammary gland

(A) Representative three immunohistochemistry for α-SMA in mammary glands of 6 M mice. Positive staining in the mammary gland stroma of *Hic1*$^{-/-}$ mice is indicated by red arrows (n = 3 for each group). **(B)** CRISPR-Cas9-mediated HIC1 deletion in MCF7 and T47D luminal BrCa cells. Cell lysates were analyzed by Western blotting with antibodies against HIC1 and GAPDH. Sg3 and sg4 represent two different interference sgRNA sequences. **(C)** Representative primary NAFs and CAFs isolated from human BrCa tissues. Western blot analysis of cell lysates was performed using antibodies against α-SMA, FAP, PDGFRα and GAPDH. **(D)** Schematic showing primary NAFs co-cultured with MCF7^{Ctrl}/MCF7^{sgHIC1} or T47D^{Ctrl}/T47D^{sgHIC1} luminal BrCa cells in a transwell apparatus (0.4 mm pore size) for 4 days. **(E)** Western blot analysis of lysates of NAF6 cells that were co-cultured with MCF7^{Ctrl}/MCF7^{sgHIC1} or T47D^{Ctrl}/T47D^{sgHIC1} luminal BrCa cells for 4 days. Antibodies against α-SMA, FAP, PDGFRα and GAPDH were used. **(F)** Immunofluorescence staining for the detection of α-SMA expression in NAF6 cells that were co-cultured with MCF7^{Ctrl}/MCF7^{sgHIC1} or T47D^{Ctrl}/T47D^{sgHIC1} luminal BrCa cells for 4 days.

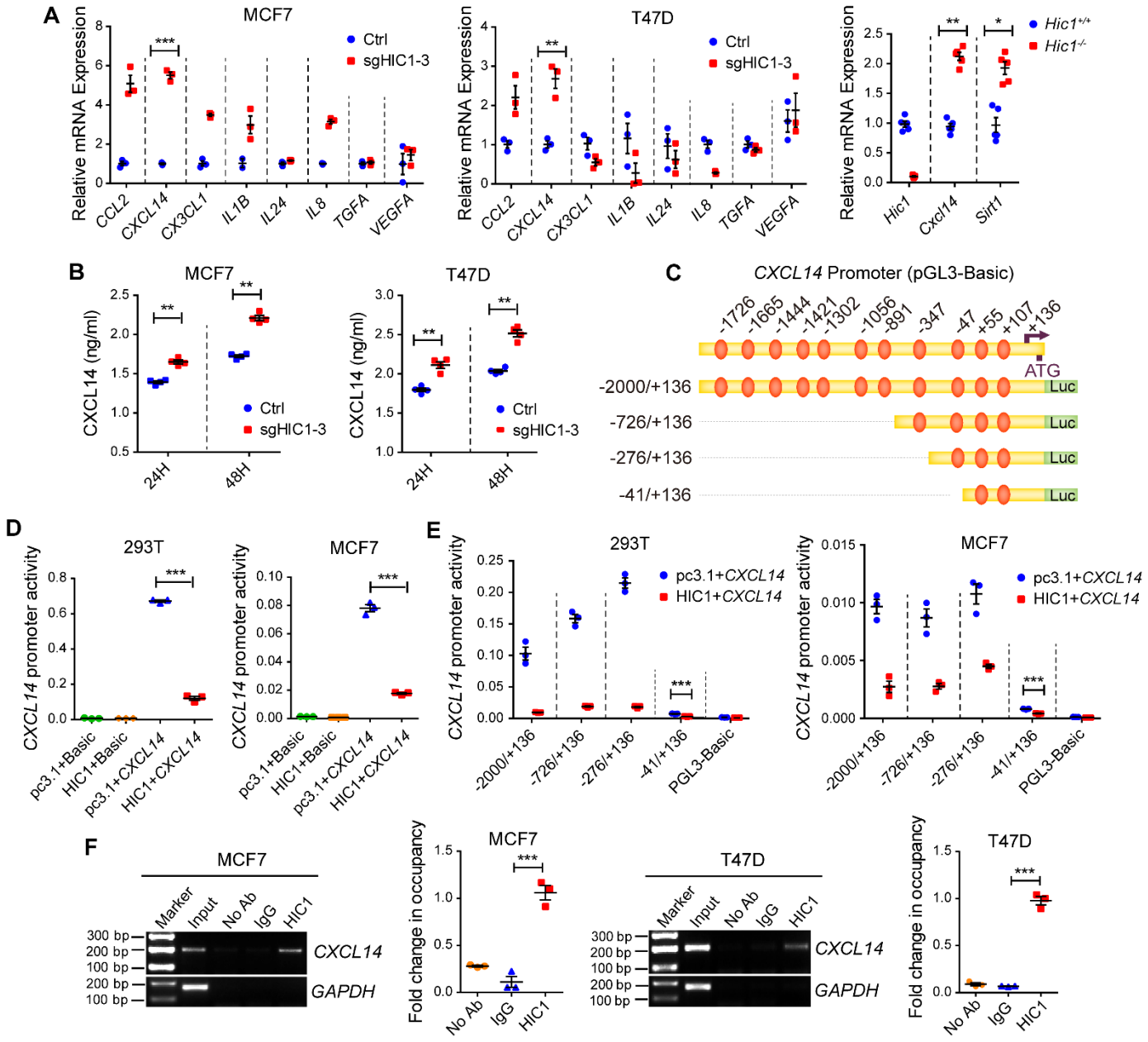

Figure 3. *CXCL14* is a direct target gene of HIC1

(A) Left: relative RT-qPCR analysis of 8 differentially expressed genes (*CCL2*, *CXCL14*, *CX3CL1*, *IL1B*, *IL24*, *IL8*, *TGFA* and *VEGFA*) after HIC1 deletion in MCF7 and T47D cells (n = 3). Right: relative RT-qPCR analysis of *Hic1*, *Cxcl14* and *Sirt1* mRNA levels in the mammary glands of *Hic1*$^{-/-}$ or *Hic1*$^{+/+}$ mice (n = 5). **(B)** ELISA analysis of CXCL14 levels in the CM of MCF7^{sgHIC1}/MCF7^{Ctrl} and T47D^{sgHIC1}/T47D^{Ctrl} cells. The supernatants were collected after culture of the cells for 24 h or 48 h (n = 4). **(C)** Schematic of the *CXCL14* promoter region. The positions of selected consensus binding sites are indicated above the diagram; the lengths of the promoter constructs used in the reporter assays are shown below. **(D)** *CXCL14* promoter activity after transfection of the full-length construct (-2000/+136) alone or together with HIC1 expression vectors. pGL3-Basic, control for promoter constructs; pc3.1, control for the HIC1 expression vector. The results are expressed as the ratio of firefly luciferase to *Renilla* luciferase (n = 3). **(E)** *CXCL14* promoter activity after co-transfection with 100 ng of the HIC1 expression vector and each of the promoter constructs. The -41/+136

construct had a significant repressive effect, despite its lower promoter activity (n = 3). **(F)** ChIP analysis of HIC1 at the *CXCL14* promoter region in MCF7 and T47D cells (n = 3) (mean ± SEM, n = 3 independent experiments; $^{*}P < 0.05$, $^{**}P < 0.01$ and $^{***}P < 0.001$; P values in A, B and E were obtained using two-tailed Student's t tests, P values in D and F were obtained using one-way ANOVA followed by Bonferroni's post-hoc test).

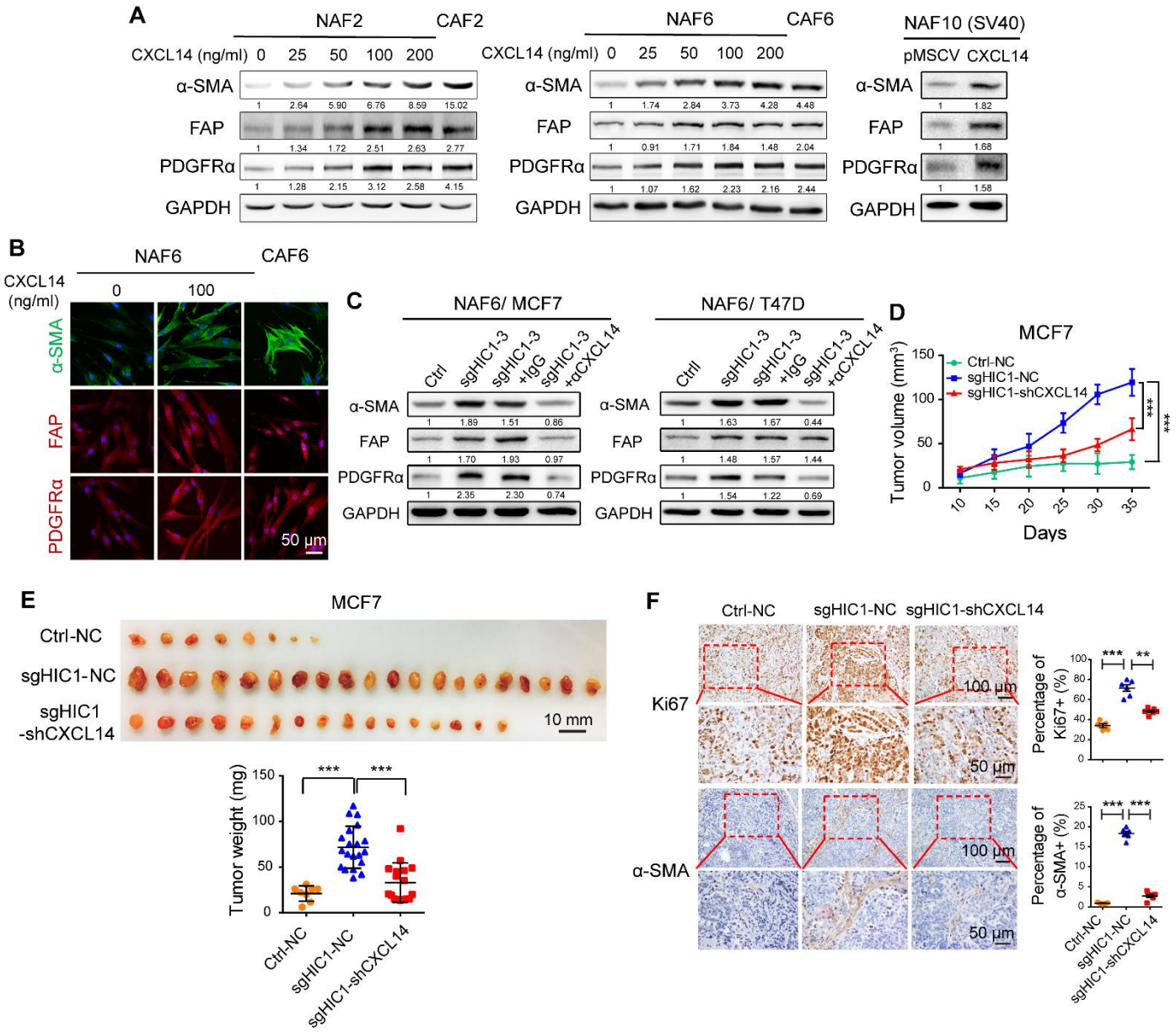

Figure 4. CXCL14 derived from HIC1-deleted BrCa cells mediates the activation of mammary fibroblasts

(A) Left: NAF2 or NAF6 cells were treated with rhCXCL14 at various concentrations (0-200 ng/ml) for 4 days. The corresponding primary CAF2 or CAF6 cells were used as positive controls. Right: the immortalized NAF10 cells stably overexpressed CXCL14. Cell lysates were analyzed by Western blotting with antibodies against α-SMA, FAP, PDGFRα and GAPDH. **(B)** Representative immunofluorescence staining detection of α-SMA, FAP and PDGFRα expression in NAF6 or CAF6 cells treated similarly to the cells described in (A). **(C)** NAF6 cells were co-cultured with $MCF7^{Ctrl}$/$MCF7^{sgHIC1}$ or with $T47D^{Ctrl}$/$T47D^{sgHIC1}$ luminal BrCa cells for 4 days in the presence or absence of an antibody against CXCL14 (α-CXCL14) at 2 μg/ml or an isotype-matched IgG control (IgG). Cell lysates from NAF6 cells were analyzed by Western blotting with antibodies against α-SMA, FAP, PDGFRα and GAPDH. **(D)** Three MCF7 cell lines (Ctrl-NC, sgHIC1-NC, sgHIC1-shCXCL14) were injected bilaterally into the fourth mammary fat pads of female BALB/c nude mice (*n* = 10

per group). Tumor volumes were measured with calipers at the indicated time points (mean ± SD; $^{***}P < 0.001$; *P* values were obtained using repeated measures ANOVA followed by a post-hoc LSD test). **(E)** Photographs and weights of the tumors obtained from the animals described in (D) (mean ± SD; $^{***}P < 0.001$, *P* values were obtained using one-way ANOVA followed by Bonferroni's post-hoc test). **(F)** Representative immunohistochemical staining for Ki67 and stromal α-SMA in tumor tissues obtained from each experimental group. The dot plots show the mean value for the percentage (%) of Ki67 or stromal a-SMA positive cells with statistical evaluation (n = 5-6) (mean ± SEM, n = 3 independent experiments; $^{**}P < 0.01$, $^{***}P < 0.001$, *P* values were obtained using one-way ANOVA followed by Bonferroni's post-hoc test).

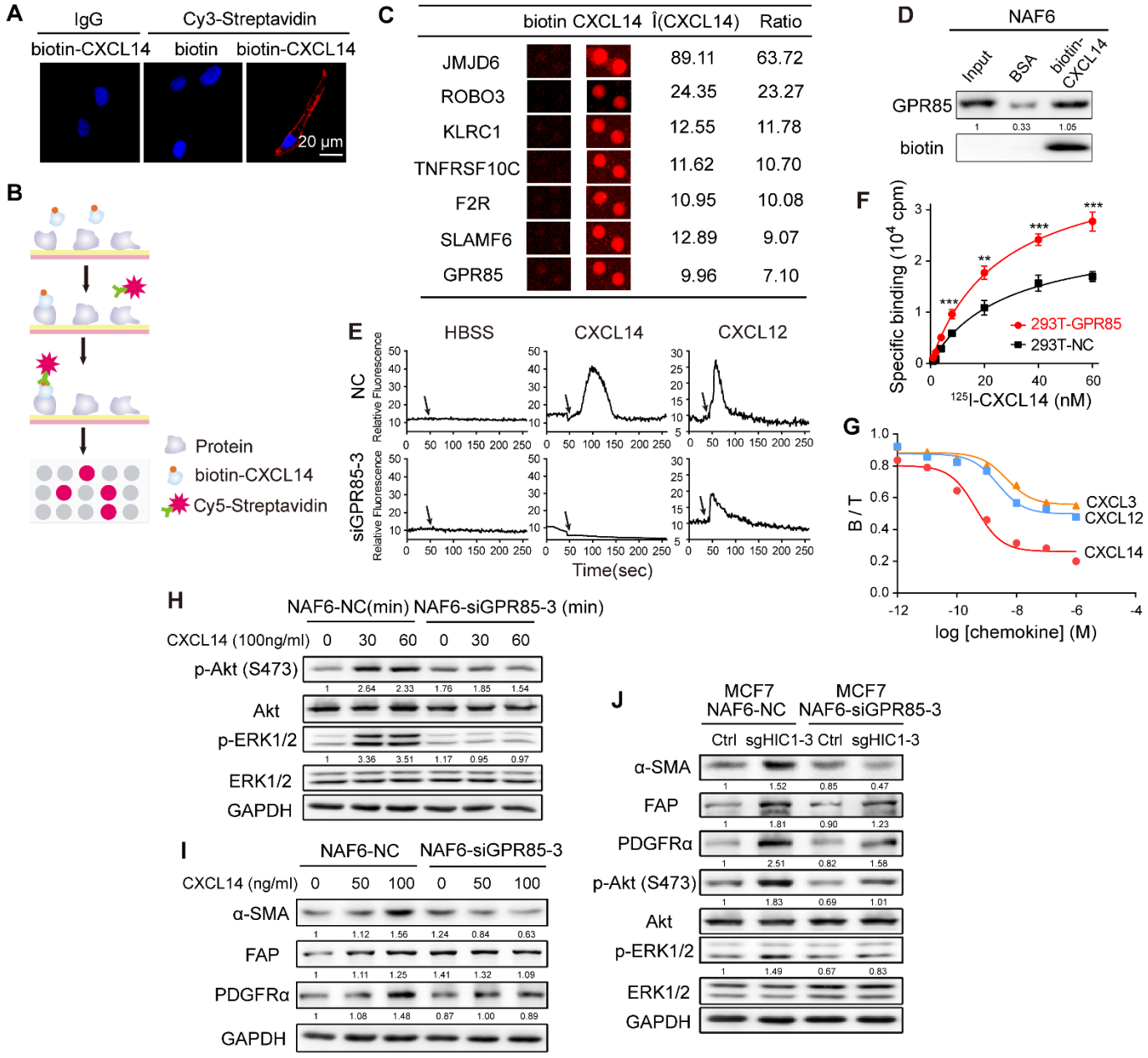

Figure 5. GPR85 is a novel functional receptor for CXCL14 activity

(A) Confocal microscopy of NAF6 cells treated with biotin or biotin-CXCL14 at 100 ng/ml at 4°C and stained with an antibody against Cy3-streptavidin. An isotype-matched IgG (IgG) was used as a control. Cell nuclei were counterstained with DAPI. **(B)** Schematic of the procedure used to detect biotin-CXCL14 binding proteins using HuProt™ human proteome microarrays containing 18,583 affinity-purified N-terminally GST-tagged proteins. **(C)** Representative CXCL14-binding membrane proteins in the proteome microarrays. **(D)** Western blotting validation using a streptavidin-agarose pulldown assay of proteome microarray determination that CXCL14 binds directly to GPR85. **(E)** Mobilization of $[Ca^{2+}]_i$ in NAF6 cells that were transfected with control siRNA (NC) or GPR85-3 siRNA and then treated with HBSS, rhCXCL14 or rhCXCL12 at 100 ng/ml. The black arrows denote the times at which stimulation was initiated. **(F)** ^{125}I-CXCL14 binding properties between 293T-NC and 293T-GPR85 cells. (mean ± SD, n = 4 repetitions; $^{**}P <$ 0.01 and $^{***}P < 0.001$; P values were obtained using two-tailed Student's t tests). **(G)** Binding assay with 10

nM of ^{125}I-CXCL14 in the presence or absence of increasing concentrations of unlabeled rhCXCL14, rhCXCL12 and rhCXCL3 for 293T cells that were transfected with GPR85. Y-axis: B/T, B represents specific binding, T represents total binding. **(H)** Knockdown of GPR85 expression by GPR85-3 siRNA in NAF6 cells in the presence or absence of rhCXCL14 at 100 ng/ml for the indicated times (0, 30 and 60 minutes). Cell lysates were analyzed by Western blotting with antibodies against p-Akt (Ser 473), Akt, p-ERK1/2, ERK1/2 and GAPDH. **(I)** Knockdown of GPR85 expression by GPR85-3 siRNA in NAF6 cells treated with rhCXCL14 at various concentrations (0-100 ng/ml) for 4 days. Cell lysates were analyzed by Western blotting with antibodies against α-SMA, FAP, PDGFRα and GAPDH. **(J)** NAF6 cells were transfected with control siRNA (NC) or GPR85-3 siRNA and then co-cultured with MCF7^{Ctrl} or MCF7^{sgHIC1} cells, respectively, for 4 days. NAF6 cell lysates were analyzed by Western blotting with antibodies against α-SMA, FAP, PDGFRα, p-Akt (Ser 473), Akt, p-ERK1/2, ERK1/2 and GAPDH.

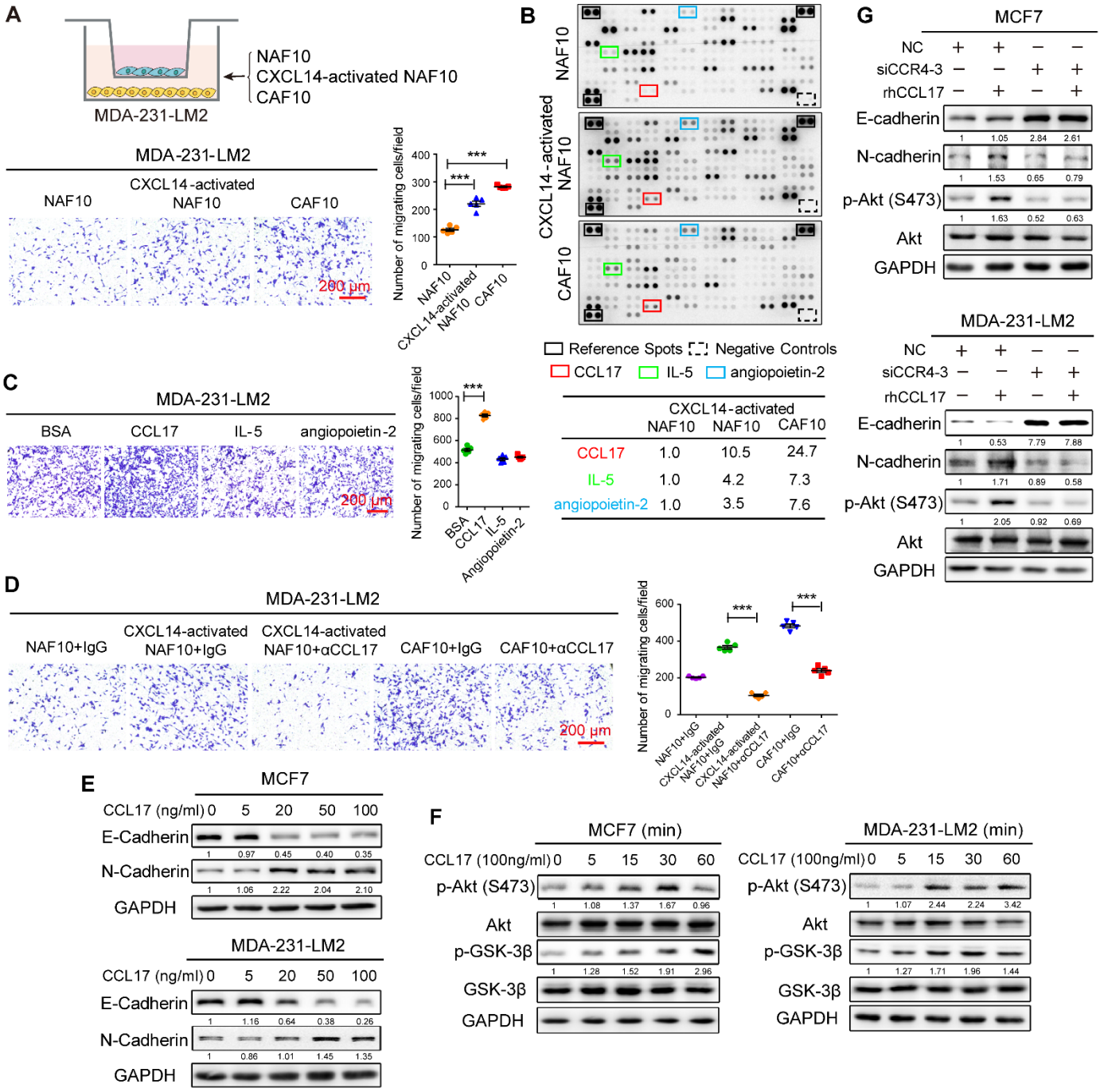

Figure 6. CXCL14-activated fibroblasts induce migration of BrCa cells via CCL17

(A) Upper: schematic showing the co-culture of MDA-231-LM2 BrCa cells with primary NAF10, CXCL14-activated NAF10 or primary CAF10 cells in a transwell apparatus (0.4 μm pore size) for 4 days. Lower: Boyden chamber assay of MDA-231-LM2 cells that were treated as above. **(B)** Upper: Human XL Cytokine Array Kits (R&D Systems) were used to measure the levels of 102 cytokines in the CM from diverse fibroblasts. Cytokines that were upregulated in the CM of CXCL14-activated NAF10 and CAF10 cells are indicated by colored boxes; they include CCL17 (red), IL-5 (green) and angiopoietin-2 (blue). The black frames indicate the positive controls, and the dashed boxes indicate the negative controls in each membrane. Lower: table showing the relative signal intensities of the three selected cytokines noted above. The signal intensities were quantified by densitometry using ImageJ software and normalized to the intensity of the

internal positive controls. **(C)** Boyden chamber assay of MDA-231-LM2 cells plated with rhCCL17, rhIL-5 and rh angiopoietin-2 in the lower chambers at 100 ng/ml for 20 hours. **(D)** Boyden chamber assay of MDA-231-LM2 cells that were co-cultured with primary NAF10, CXCL14-activated NAF10 or primary CAF10 cells in a transwell apparatus for 4 days in the presence or absence of an antibody against CCL17 (α-CCL17, 1 μg/ml) or an isotype-matched IgG control (IgG). **(E)** MCF7 or MDA-231-LM2 cells were treated with various concentrations (0-100 ng/ml) of rhCCL17 for 4 days, and lysates of the cells were analyzed by Western blotting using antibodies against E-cadherin, N-cadherin and GAPDH. **(F)** MCF7 or MDA-231-LM2 cells were treated with rhCCL17 at 100 ng/ml for the indicated times (0, 5, 15, 30 and 60 minutes). Cell lysates were analyzed by Western blotting with antibodies against p-Akt (Ser 473), Akt, p-GSK-3β (Ser9), GSK-3β and GAPDH. **(G)** Knockdown of CCR4 expression by siRNA-3 in MCF7 and MDA-231-LM2 cells in the presence or absence of rhCCL17 at 100 ng/ml for 4 days. Cell lysates were analyzed by Western blotting with antibodies against E-cadherin, N-cadherin, p-Akt (Ser 473), Akt and GAPDH. (mean ± SEM, n = 3 independent experiments; $^{***}P < 0.001$, P values were obtained using one-way ANOVA followed by Bonferroni's post-hoc test).

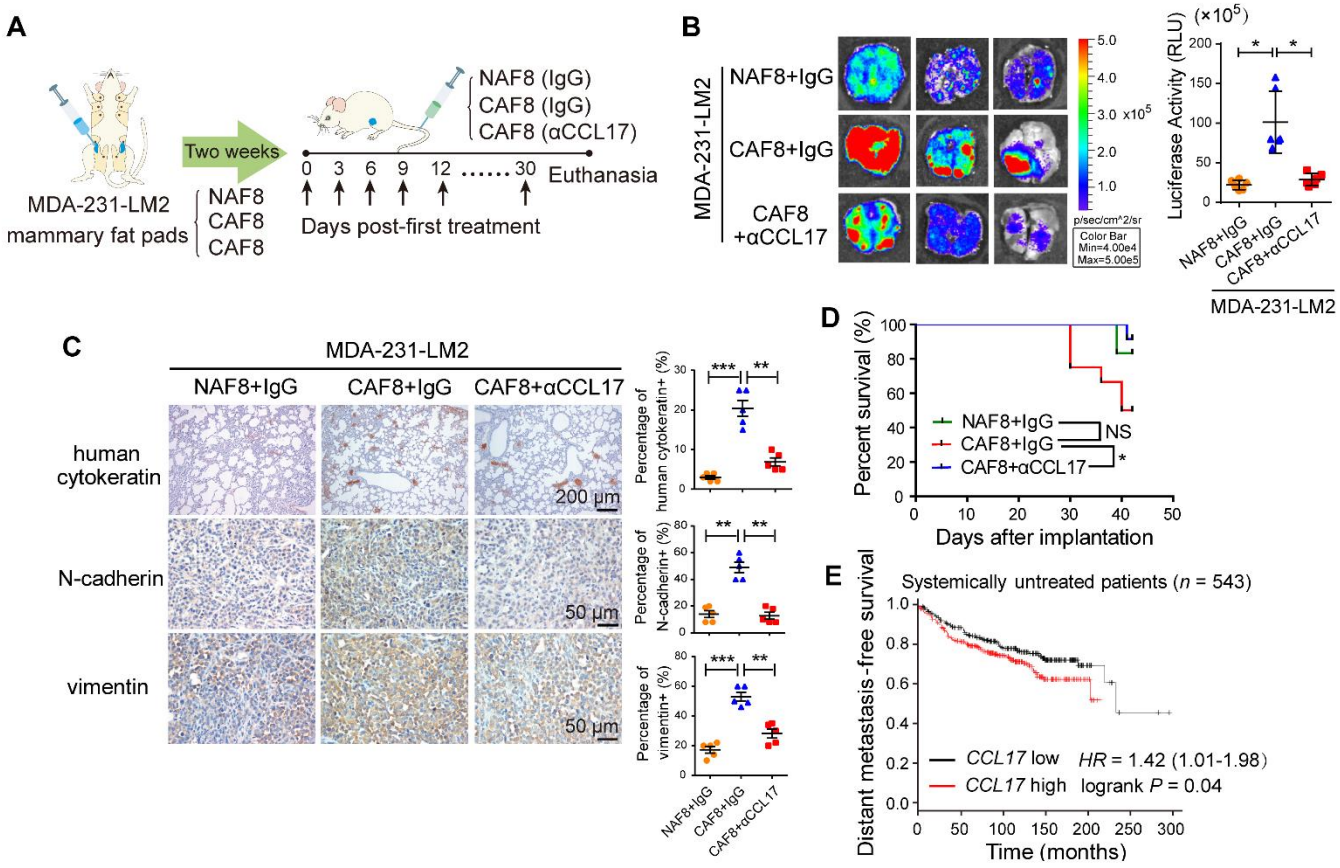

Figure 7. CCL17 secreted by CAFs promotes lung metastasis of BrCa xenografts

(A) Schematic showing the lung metastasis model of breast cancer xenografts. MDA-231-LM2 BrCa cells mixed with primary NAF8 or CAF8 cells at a ratio of 3:1 were implanted bilaterally into the mammary fat pads of BALB/c nude mice (n = 12 per group). When the xenografts became palpable two weeks later, control IgG or a neutralizing antibody against CCL17 (αCCL17, 1 μg/mouse) was then injected via the tail vein every three days for thirty days; the mice were then euthanized. **(B)** Representative bioluminescence imaging of the harvested lungs (left) and quantification of their bioluminescent signals (right, n = 6) (mean ± SD; $^{*}P < 0.05$, P values were obtained using one-way ANOVA followed by Bonferroni's post-hoc test). **(C)** Representative immunohistochemical staining for human cytokeratin of each group's lung tissues and for N-cadherin and vimentin in orthotopic xenografts. The dot plots show the mean values for the percentage (%) of human cytokeratin-, N-cadherin- or vimentin-positive cells with statistical evaluation (n = 5) (mean ± SEM, n = 3 independent experiments; $^{**}P < 0.01$ and $^{***}P < 0.001$, P values were obtained using one-way ANOVA followed by Bonferroni's post-hoc test). **(D)** Kaplan-Meier survival curves of BALB/c nude mice that received the indicated treatments (NS, not significant; $^{*}P < 0.05$; P values were obtained using the log-rank test). **(E)** Kaplan-Meier plots of distant metastasis-free survival (DMFS) of systemically untreated patients (n = 543) stratified by *CCL17* expression. The data were obtained from the Kaplan-Meier plotter database (P = 0.04; P values were obtained using the log-rank test) (27).

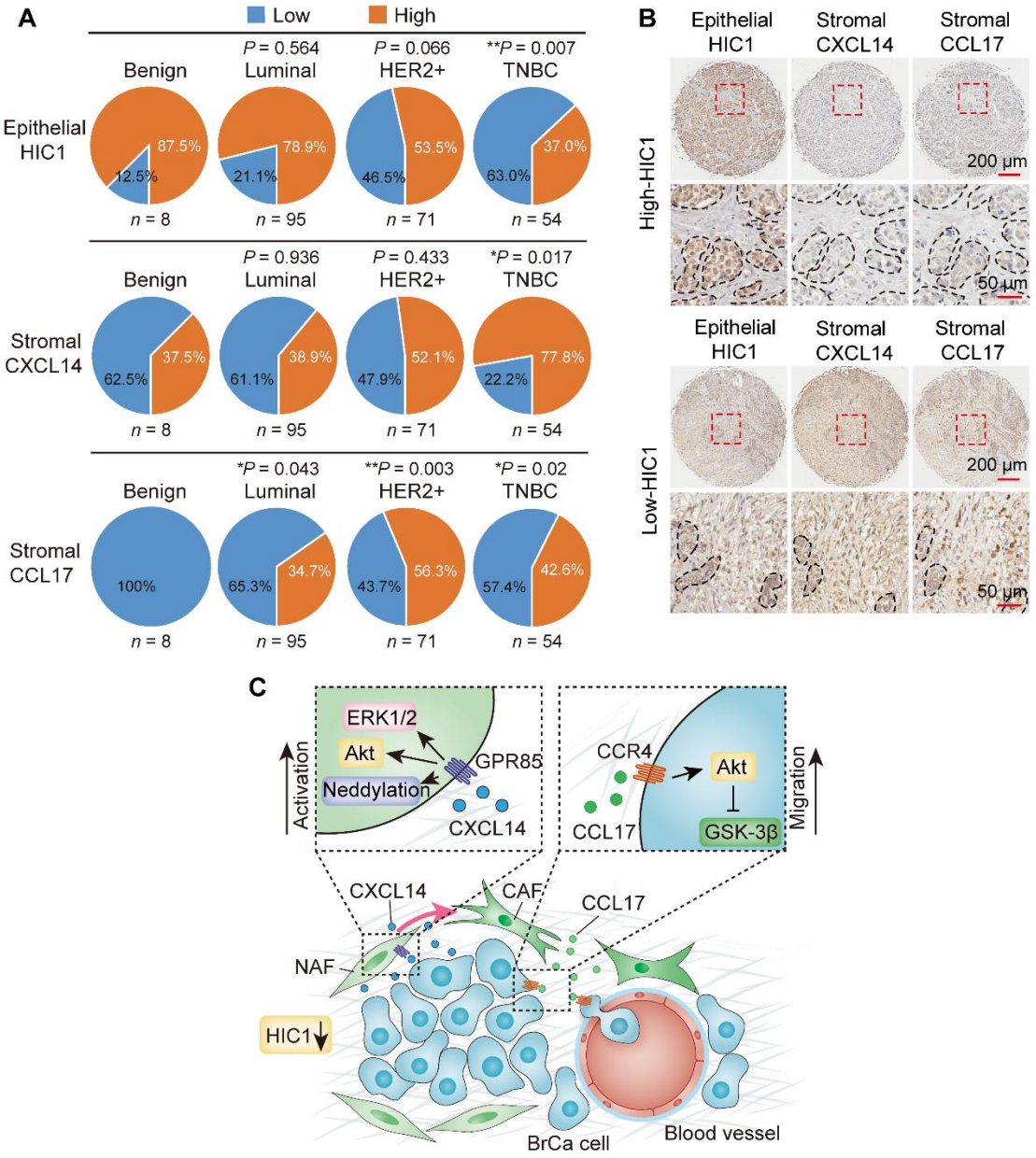

Figure 8. The HIC1-CXCL14-CCL17 loop is associated with malignant progression in BrCa patients

(A) The percentages of low and high expression of epithelial HIC1 (upper), stromal CXCL14 (middle) and stromal CCL17 (bottom) in benign breast tissue and various breast cancer subtypes are shown as a pie chart (*P vs* benign; *P* values were obtained using the Chi-square test). **(B)** Representative IHC images showing the correlation between epithelial HIC1 expression and stromal CXCL14/CCL17 expression in 228 benign and malignant breast tumor samples. The broken lines indicate the margins of the tumor. **(C)** Schematic model showing how HIC1-mediated crosstalk between cancer cells and mammary fibroblasts promotes BrCa progression. Conditional deletion of HIC1 in the mouse mammary gland may contribute to premalignant transformation at the early stage of breast tumor formation. Moreover, chemokine CXCL14 secreted by HIC1-deleted BrCa cells binds to its cognate receptor GPR85 on mammary fibroblasts in the microenvironment, thereby activating the fibroblasts through the ERK1/2, Akt, and neddylation pathways. The activated fibroblasts in turn promote BrCa progression through induction of EMT by activation of the CCL17/CCR4

chemokine axis.

Table 1. Spearman's rank correlation coefficient analysis of protein expression in 228 benign and malignant breast tumor samples

Variables		HIC1 (Epithelial)	CXCL14 (Stromal)	CCL17 (Stromal)
HIC1 (Epithelial)	Spearman (*r*)	1	-0.254	-0.072
	P value	-	<0.001	0.277
CXCL14 (Stromal)	Spearman (*r*)	-0.254	1	0.300
	P value	<0.001	-	<0.001
CCL17 (Stromal)	Spearman (*r*)	-0.072	0.300	1
	P value	0.277	<0.001	-

$r > 0$, positive correlation; $r < 0$, negative correlation.